

Quantum property preservation

Kumar Saurav^{1,2} and Daniel A. Lidar^{1,2,3,4}

¹*Center for Quantum Information Science & Technology*

²*Department of Electrical & Computer Engineering*

³*Department of Physics & Astronomy*

⁴*Department of Chemistry*

University of Southern California, Los Angeles, CA 90089, USA

Quantum property preservation (QPP) is the problem of maintaining a target property of a quantum system for as long as possible. This problem arises naturally in the context of open quantum systems subject to decoherence. Here, we develop a general theory to formalize and analyze QPP. We characterize properties encoded as scalar functions of the system state that can be preserved time-locally via continuous control using smoothly varying, time-dependent control Hamiltonians. The theory offers an intuitive geometric interpretation involving the level sets of the target property and the stable and unstable points related to the noise channel. We present solutions for various noise channels and target properties, which are classified as trivially controllable, uncontrollable, or controllable. In the controllable scenario, we demonstrate the existence of control Hamiltonian singularities and breakdown times, beyond which property preservation fails. QPP via Hamiltonian control is complementary to quantum error correction, as it does not require ancilla qubits or rely on measurement and feedback. It is also complementary to dynamical decoupling, since it uses only smooth Hamiltonians without pulsing and works in the regime of Markovian open system dynamics. From the perspective of control theory, this work addresses the challenge of tracking control for open quantum systems.

I. INTRODUCTION

Quantum control is the generalization of the well-established classical control theory to the quantum domain, dating back at least to the early 1980s [1, 2]. The field has since expanded greatly into mathematics [3], physics [4, 5], chemistry [6, 7], and quantum technology [8]. In the context of quantum information and computation, quantum control is often used to design improved quantum logic gates [9–14]. It has long been recognized that quantum error correction can be viewed as a quantum control problem as well [15–18].

Much of the work in quantum control to date has been devoted to questions of controllability and optimal state-to-state or operator-to-operator transformations. Here, we introduce the complementary problem of *quantum property preservation* (QPP). We define this task more precisely below, but in essence, it amounts to selecting an arbitrary function of the quantum state and preserving its initial value in the presence of a decohering environment [19, 20]. QPP is less demanding than full state or operator preservation but is nevertheless of fundamental and practical interest.

The fundamental interest in QPP arises in the context of understanding the limits of what can be preserved in a restricted and minimalistic scenario where the only resource available is *smooth Hamiltonian control*. Namely, unlike in quantum error avoidance [21, 22] or correction [23–25], we explicitly avoid introducing any encoding or measurement-based feedback, whether classical or coherent [26]. Moreover, the only control we allow is a smooth, time-dependent Hamiltonian that preserves the property time-locally, i.e., we avoid the “bang-bang” control setting of dynamical decoupling [27–29], which only

recovers a state at the end of each decoupling cycle and only applies under non-Markovian dynamics. We note that the general theory of quantum error correction and suppression already provides a framework that allows for (stroboscopic) QPP as a special case [30–32]. By excluding the resources assumed by the former, preserving an arbitrary quantum state becomes impossible, but, as we show here, it remains possible to preserve specific properties of quantum states.

The practical interest in QPP without encoding or feedback and using only smooth controls arises, in part, from its very minimalism. It also arises naturally in situations where it is possible to precompute a stabilizing state trajectory so that a given property can be preserved over time as intended. When this is the case, the control Hamiltonian (which becomes a function of the instantaneous system state) can be implemented without requiring continuous state tracking. While we do not discuss specific applications here, this is a relevant scenario for, e.g., metrology and sensing, where QPP can demonstrate an advantage [33]. Some examples of critical quantum properties to preserve in an open system setting are coherence, fidelity, mean energy, or, more generally, any expectation value.

More formally, the main questions we address in this work are the following: (1) Which class of properties $f(\rho)$ can be preserved given a decohering environment, where f is the desired (scalar) function of the instantaneous state ρ ? (2) Given a property f , what control Hamiltonian needs to be applied to preserve $f(\rho)$ over a specified evolution period? (3) How long can this period be? (4) What is the underlying geometry of the control landscape? We consider these questions in both the general setting of finite-dimensional Hilbert spaces and in the

special case of a single qubit, where the underlying geometry can be visualized intuitively.

The QPP problem we have defined can be placed within the framework of *tracking control*, which has a rich history in classical control theory [34–36]. It was extensively studied in the context of closed quantum systems [37–42].

This work is organized as follows. Section II provides the background and notation, and develops the general theory for arbitrary Hilbert spaces. Section III specializes these ideas in the qubit setting. Examples for two selected properties (coherence and fidelity) and different noise channels are discussed in Section IV. Section V concludes. Additional technical details are provided in the Appendix.

II. THEORY AND METHODS

A. Background

The most general form of a time-local master equation governing the dynamics of open quantum systems described by a state (density matrix) $\rho(t)$ is [19, 20]:

$$\dot{\rho} = \mathcal{L}(\rho) = \mathcal{L}_H(\rho) + \mathcal{L}_D(\rho) \quad (1a)$$

$$\mathcal{L}_H(\rho) = -i[H, \rho] \quad (1b)$$

$$\mathcal{L}_D(\rho) = \sum_{\alpha} \gamma_{\alpha}(t)(L_{\alpha}\rho L_{\alpha}^{\dagger} - \frac{1}{2}\{L_{\alpha}^{\dagger}L_{\alpha}, \rho\}), \quad (1c)$$

where where the dot denotes $\partial/\partial t$, \mathcal{L} is the Liouvillian, \mathcal{L}_D the dissipator, and the unitary dynamics are generated by \mathcal{L}_H . We allow both \mathcal{L}_D and \mathcal{L}_H to be time-dependent, either explicitly or implicitly. When the rates $\gamma_{\alpha}(t) \geq 0 \forall \alpha$ the dynamics are Markovian; otherwise the master equation describes general non-Markovian, time-local dynamics [43–45]. We nevertheless refer to the L_{α} as Lindblad operators (even in the non-Markovian case) and assume that they are traceless, such that the traceful part is absorbed into the Hamiltonian H .

In the tracking control setting, we view H as the control Hamiltonian $H[\rho(t)]$, which is allowed to depend on the instantaneous state $\rho(t)$ of the system, i.e., an implicit time dependence. Here, we do not consider the complications associated with measuring the state and the inevitable delay in making H dependent upon the measurement result. In this sense, the results we present in this work are upper bounds on the achievable performance of tracking control. Alternatively, the predicted performance can be realized in cases where the Hamiltonian can be precomputed.

We consider a finite-dimensional Hilbert space \mathcal{H} with $d = \dim(\mathcal{H}) < \infty$, and the space of bounded linear operators $\mathcal{B}(\mathcal{H})$ acting on \mathcal{H} equipped with the Hilbert-Schmidt inner product $\langle A, B \rangle \equiv \text{Tr}(A^{\dagger}B)$. Quantum states are represented by density operators $\rho \in \mathcal{B}_+(\mathcal{H})$ (positive trace-class operators acting on \mathcal{H}) with unit trace: $\text{Tr}\rho = 1$. A *nice operator basis* for \mathcal{H} is a set of

orthonormal Hermitian operators $\{F_j\}_{j=0}^J \in \mathcal{B}(\mathcal{H})$ such that $F_0 \propto I$ where I is the identity operator. Consequently, $F_0 = \frac{1}{\sqrt{d}}I$, $\langle F_j, F_k \rangle = \delta_{jk}$ and for $j \geq 1$ the operators F_j are traceless.

Expanding the state in the nice operator basis yields $\rho(t) = \frac{1}{d}I + \sum_{j=1}^J v_j(t)F_j$, where the *coherence vector* $\mathbf{v} \in \mathcal{M}^{(d)} \subset \mathbb{R}^J$ has coordinates given by $v_j = \langle F_j, \rho \rangle$, and $J \equiv d^2 - 1$. $\mathcal{M}^{(d)}$ is a convex set that is topologically equivalent to a sphere [46]; see Appendix A for more details. The coherence vector completely characterizes the state, and instead of working in $\mathcal{B}(\mathcal{H})$ we can equivalently work in \mathbb{R}^J with the standard Euclidian inner product $\mathbf{a} \cdot \mathbf{b} = \mathbf{a}^T \mathbf{b} = \mathbf{b}^T \mathbf{a} = \sum_j a_j b_j$. Rewriting Eq. (1) in matrix form for the coherence vector gives:

$$\dot{\mathbf{v}} = (Q + R)\mathbf{v} + \mathbf{c}, \quad (2)$$

where Q and R are the matrices corresponding to \mathcal{L}_H and \mathcal{L}_D , respectively, and \mathbf{c} is non-zero only in the non-unital case [i.e., when $\mathcal{L}_D(I) \neq 0$], and depends purely on \mathcal{L}_D . All the vectors and matrices in Eq. (2) are real-valued. Moreover, Q is anti-symmetric, and R is symmetric when $d = 2$ (qubit) or when the Lindblad operators are all Hermitian [47]. In the context of the coherence vector, we refer to Q as the control matrix and refer to $D \equiv (R, \mathbf{c})$ as the dissipator, since both R and \mathbf{c} depend only on \mathcal{L}_D . Note that in the tracking control setting, $Q = Q(\mathbf{v})$, i.e., the control depends on the state. We use both the density operator and coherence vector formalisms below, emphasizing one over the other as convenient.

B. Realizable trajectories

We refer to differentiable operators from a non-empty interval of the real numbers to $\mathcal{B}_+(\mathcal{H})$ as *trajectories* and solutions of Eq. (2) with a given Hamiltonian H as *H-realizable trajectories*. We assume throughout that $\|H\| < \infty$, where the norm can be chosen as needed to reflect desirable physical constraints, such as a maximum power constraint. Denoting the set of H -realizable trajectories by \mathbb{P}_H , the set \mathbb{P} of *realizable trajectories* is then the union of the sets \mathbb{P}_H .

Alternatively, from a control theory perspective, we can start from a given realizable trajectory ρ , agnostic of the control that realizes it. Then, an equivalent definition is:

$$\mathbb{P} = \{\rho(\cdot) : \exists H(\cdot) \text{ s.t. } \rho, H \text{ satisfy Eq. (1)}\} \quad (3)$$

Proof. Let $\cup \mathbb{P}_H = \mathbb{P}^1$ and denote the set in Eq. (3) by \mathbb{P}^2 . If $\rho \in \mathbb{P}^1$, then $\rho \in \mathbb{P}_H$ for some H . By definition, the pair (ρ, H) satisfies Eq. (1) and therefore $\rho \in \mathbb{P}^2$. This proves $\mathbb{P}^1 \subseteq \mathbb{P}^2$. Now suppose $\sigma \in \mathbb{P}^2$. By definition, for some H , (σ, H) satisfies Eq. (1), which means $\sigma \in \mathbb{P}_H$. Therefore $\sigma \in \mathbb{P}^1$. So $\mathbb{P}^2 \subseteq \mathbb{P}^1$. \square

Note that using the nice operator basis, realizable trajectories, which are density matrix solutions of Eq. (1),

map bijectively to coherence vector solutions of Eq. (2). Based on convenience, we will alternate between these two possible representations of solutions, and refer to both as realizable trajectories.

We will require the following notion of equivalence of trajectories:

Definition 1. *Two trajectories, $\rho_1 : I_1 \mapsto \mathcal{B}_+(\mathcal{H})$ and $\rho_2 : I_2 \mapsto \mathcal{B}_+(\mathcal{H})$ are said to be equivalent iff there exists a bijective continuously differentiable map $\varphi : I_1 \mapsto I_2$ such that $\forall t \in I_1$: (1) $\rho_1(t) = \rho_2(\varphi(t))$ and (2) $\varphi'(t) > 0$.*

From hereon, we use the notation $\sigma(u)$ to denote a trajectory in $\mathcal{B}_+(\mathcal{H})$ and $\mathbf{l}(u)$ to denote a trajectory in $\mathcal{M}^{(d)}$, both parametrized by $u \in I_1 = [0, 1]$. We reserve the notation $\rho(t)$ and $\mathbf{v}(t)$ to denote the density matrix and coherence vector parametrized by time $t \in I_2 = [0, t_f]$, where t_f denotes the final time. The map $\varphi : I_1 \mapsto I_2$ transforms the dimensionless parameter u to time t .

C. General tracking control framework

The target function can be described as a scalar function of the system state ρ , which can be written as $f[\rho(t)]$, but we suppress the explicit time-dependence from here on. We assume throughout this work that the function f is real-valued and differentiable. An example is the state purity $f(\rho) = \text{Tr}\rho^2 \equiv P(\rho)$. The gradient of the scalar function f is:

$$\nabla f(\rho) = \sum_{j=1}^J \frac{\partial f}{\partial v_j} F_j. \quad (4)$$

where \mathbf{v} is the coherence vector for ρ and F_j are the basis elements in the nice operator basis. Note that since f is real-valued, the coefficients of ∇f in the nice operator basis are real, and therefore, the $d \times d$ traceless matrix on the r.h.s. of Eq. (4) is Hermitian. This representation of ∇f is appropriate when it is considered an operator in $\mathcal{B}(\mathcal{H})$, in combination with the density operator. Equivalently, $\nabla f = (\frac{\partial f}{\partial v_1}, \dots, \frac{\partial f}{\partial v_J})$ is a vector in \mathbf{R}^J , which is appropriate when it is considered in combination with the coherence vector. Both representations are used below, and the appropriate representation will be clear by context.

The goal of time-local QPP is to keep the target property constant for as long as possible, i.e., to find a control Hamiltonian such that $f[\rho(t)] = f[\rho(0)]$ for all $t \in [0, t_f]$, while maximizing t_f . This is equivalent to $\frac{d}{dt} f[\rho(t)] = 0$ for all $t \in [0, t_f]$, i.e.:

$$\langle \nabla f, \dot{\rho} \rangle = 0 = \nabla f \cdot \dot{\mathbf{v}}. \quad (5)$$

Here, on the l.h.s. $\nabla f \in \mathcal{B}(\mathcal{H})$ while on the r.h.s. $\nabla f \in \mathbf{R}^J$.

Any function f independent of ρ is trivially preservable since $\nabla f = 0$ in Eq. (5). For the rest of this work, we only

consider non-trivial functions f with a non-zero gradient over $\mathcal{B}_+(\mathcal{H})$.

Eq. (5) formalizes that to preserve f , the path of the coherence vector should be restricted to the *level set* of f , i.e., the hypersurface on which f is constant (recall that if f is differentiable, then ∇f at a point is either orthogonal to the level set of f at that point or zero).

Therefore, the equations that govern the tracking control problem are the *dynamics equation* Eq. (1) for the density matrix or Eq. (2) for the coherence vector, along with the respective forms of the *constraint equation*

$$\langle \nabla f, -i[H, \rho] + \mathcal{L}_D \rho \rangle = 0 \quad (6a)$$

$$\nabla f \cdot [(Q + R)\mathbf{v} + \mathbf{c}] = 0. \quad (6b)$$

Note that in the tracking control problem setting, the control Hamiltonian H and Q are explicit functions of $\rho(t)$ and $\mathbf{v}(t)$, respectively, instead of t .

Definition 2. *For a given target property f , a control Hamiltonian H for which the constraint equation is satisfied, is called an f -preserving Hamiltonian.*

Definition 3. *A solution of the dynamics and constraint equations for $t \in [0, t_f]$ is called an f -preserving trajectory $\rho(t)$ [or $\mathbf{v}(t)$].*

D. Uncontrollable and trivially controllable target properties

Two exceptional cases of target properties arise from the constraint equation, which we call trivially controllable and uncontrollable.

1. Trivially controllable f

Definition 4. *A target property f is trivially controllable when for all ρ*

$$\langle \nabla f, \mathcal{L}_D \rho \rangle = 0 = \nabla f \cdot (R\mathbf{v} + \mathbf{c}). \quad (7)$$

This holds when the dissipator itself moves the state along the level set of f . In this case, f is already invariant under the action of the dissipator, and an additional control Hamiltonian is not needed to preserve it, i.e., we can set $H = Q = 0$.

As a simple example that we will use throughout to illustrate the theory, consider:

Example 1: Markovian dephasing of a single qubit: $L_\alpha = \sigma^z$ and $\gamma_\alpha(t) = \gamma$ in Eq. (1c). Equivalently, $R = \text{diag}(-2\gamma, -2\gamma, 0)$ and $\mathbf{c} = 0$.

In this case, any target property f for which $\nabla f \cdot R\mathbf{v} = \frac{\partial f}{\partial v_x} v_x + \frac{\partial f}{\partial v_y} v_y = 0$ is trivially controllable. One solution of this partial differential equation is $f(\mathbf{v}) = f(v_z)$. Another solution is any target property that depends only on the ratio v_y/v_x , i.e., $f(\mathbf{v}) = g(v_y/v_x)$, where g is an arbitrary function.

2. Uncontrollable f

Definition 5. A target property f is uncontrollable when it is not trivially controllable and

$$\langle \nabla f, -i[H, \rho] \rangle = \langle H, -i[\rho, \nabla f] \rangle = 0, \quad (8)$$

whenever $\langle \nabla f, \mathcal{L}_D \rho \rangle \neq 0$.

We impose that f is not trivially controllable since otherwise, we cannot guarantee the existence of a ρ such that $\langle \nabla f, \mathcal{L}_D \rho \rangle \neq 0$.

For a given state ρ , the uncontrollability condition (8) holds for all control Hamiltonians iff $i[\rho, \nabla f] = 0$. At such points, any change in the target property value f depends solely on the dissipator, and the control Hamiltonian has no effect.

In terms of the coherence vector, uncontrollable target properties are equivalently characterized by

$$\nabla f \cdot Q\mathbf{v} = (\nabla f)^T Q\mathbf{v} = -\mathbf{v}^T Q \nabla f = 0, \quad (9)$$

whenever $\nabla f \cdot (R\mathbf{v} + \mathbf{c}) = (\nabla f)^T (R\mathbf{v} + \mathbf{c}) \neq 0$, using the antisymmetry of Q and the symmetry of the dot product over real vector spaces. Eq. (9) holds for all Q iff $\nabla f \propto \mathbf{v}$.

Proposition 1. Any target property that depends only on the magnitude $v \equiv \|\mathbf{v}\|$ of the coherence vector, and for which $\mathbf{v}^T (R\mathbf{v} + \mathbf{c}) \neq 0$, is uncontrollable.

Proof. For this class of properties $f(\mathbf{v})$ can be written as a scalar function $f(v)$, so that:

$$\nabla f(\mathbf{v}) = \nabla f(v) = \frac{df(v)}{dv} \frac{\mathbf{v}}{v} \propto \mathbf{v}. \quad (10)$$

Then $(\nabla f)^T Q\mathbf{v} = -\mathbf{v}^T Q \nabla f$ implies $\mathbf{v}^T Q\mathbf{v} = 0$ and Eq. (9) holds. The property $(\nabla f)^T (R\mathbf{v} + \mathbf{c}) \neq 0$ holds by assumption. \square

Example 2: An example of an uncontrollable target property is the purity: $P(\rho) = \frac{1}{d} + v^2$. In the case of Markovian dephasing (Example 1), $R\mathbf{v}' + \mathbf{c} \neq \mathbf{0}$ for states $\mathbf{v}' \neq (0, 0, v_z)$. For any such \mathbf{v}' , Eq. (9) holds.

3. Controllable target properties

Having defined and characterized trivially controllable and uncontrollable target properties, we now define:

Definition 6. A controllable target property is a target property that is neither trivially controllable nor uncontrollable.

An example of a controllable target property is coherence preservation subject to dephasing, as discussed below, in Section IV A.

E. f -preserving Hamiltonians for controllable target properties

Next, we identify necessary conditions f -preserving Hamiltonians must satisfy when a target property is controllable.

Theorem 1. An f -preserving control Hamiltonian satisfies

$$\langle H, i[\rho, \nabla f] \rangle = \langle \nabla f, \mathcal{L}_D \rho \rangle. \quad (11)$$

Assuming $[\rho, \nabla f] \neq 0$, a particular (but not unique) solution of Eq. (11) is:

$$H = i \frac{\langle \nabla f, \mathcal{L}_D \rho \rangle}{\|[\rho, \nabla f]\|^2} [\rho, \nabla f]. \quad (12)$$

Proof. Eq. (11) follows directly from rearranging Eq. (6a) using the identity $\langle \nabla f, i[H, \rho] \rangle = \langle H, i[\rho, \nabla f] \rangle$. Eq. (12) satisfies Eq. (11) by inspection. \square

Note that, based on Eq. (12), the overall scale of f cancels out, and the f -preserving component of the control Hamiltonian is linear in the dissipator.

Using Definition 3 of an f -preserving trajectory, we can now state that such trajectories arise in particular when the system evolution is obtained by applying a control Hamiltonian which obeys Eq. (11).

It is clear that trivially controllable target properties correspond to Eq. (11) being satisfied with $H = 0$ for all states ρ . Likewise, uncontrollable target properties correspond to the l.h.s. of Eq. (11) vanishing with the r.h.s. remaining non-zero. In Eq. (12), uncontrollable target properties correspond to H diverging. We call a state and a time at which this happens a *breakdown point* and *breakdown time*, respectively, and return to these concepts in Section II G.

1. Geometric interpretation

Eq. (11) has a geometric interpretation: the dissipator can cause the state to move away from the level set, and since ∇f is orthogonal to the level set, this is quantified by the magnitude of $\langle \nabla f, \mathcal{L}_D \rho \rangle$ or $\nabla f \cdot (R\mathbf{v} + \mathbf{c})$. The control Hamiltonian can also push ρ away from the level set; however, its action is *orthogonal* to ρ (since they appear together in a commutator, akin to the vector product; see Section III A). Therefore, to counteract the dissipator, the relevant Hamiltonian component is the one that is orthogonal to both ρ and ∇f (i.e., $\langle H, i[\rho, \nabla f] \rangle$), and the required magnitude is the same as that given by the dissipator.

2. Control parameters

The d^2 matrix elements of H in a nice operator basis are the *control parameters*. We call a control parameter

relevant when it is needed for satisfying the constraint Eq. (11). Next, we address how many control parameters are relevant.

Proposition 2. *Let m_0 denote the multiplicity of the 0 eigenvalue of $i[\rho, \nabla f]$; then H has exactly $d - m_0$ relevant control parameters with which to satisfy the constraint Eq. (11). In particular, the number of relevant control parameters is at most d .*

Proof. The operator $i[\rho, \nabla f]$ is Hermitian and has a spectral decomposition. After diagonalization it can be written as $\sum_{j=0}^{d-1} \beta_j |\beta_j\rangle\langle\beta_j|$. In the same basis, H can be expanded as $\sum_{j,k=0}^{d-1} h_{jk} |\beta_j\rangle\langle\beta_k|$. Thus, Eq. (11) becomes:

$$\sum_{j=0}^{d-1} h_{jj} \beta_j = \langle \nabla f, \mathcal{L}_D \rho \rangle. \quad (13)$$

This is a linear equation involving scalars on both sides. Since m_0 is the number of zero β_j 's, the sum on the l.h.s. is over the $d - m_0$ terms for which $\beta_j \neq 0$. The corresponding h_{jj} are the relevant control parameters for satisfying the constraint Eq. (11). \square

Note that the remaining $d^2 - (d - m_0)$ control parameters in H are irrelevant to time-local property preservation, i.e., they play no role in satisfying Eq. (11). However, in practice, it may be advantageous to utilize these control parameters as well (instead of setting them to zero) if this simplifies the implementation of the control Hamiltonian. Moreover, modifying these parameters can also change the breakdown time (e.g., see Section IV A 3).

F. Stable points

The goal of preserving the target property for as long as possible motivates the following definition:

Definition 7. *A stable point of a given dissipator is a system state ρ for which the control Hamiltonian can be chosen so that ρ , and hence any target property, is indefinitely preserved, i.e., $\dot{\rho} = 0 \forall t$.*

Note that this definition is closely related to the concept of decoherence-free subspaces in the Markovian setting [48, 49], but unlike the latter, we do not assume the availability of additional qubits for encoding.

The converse of a stable point is:

Definition 8. *A unstable point is a system state ρ for which $\dot{\rho} \neq 0$ for all control Hamiltonians H .*

Under an appropriate control, the system state does not change when it is at a stable point, and therefore, neither does the purity $P(\rho) = \text{Tr}\rho^2$. However, a constant purity is not a sufficient condition for stable points:

Proposition 3. *For $d > 2$, $\dot{P} = 0$ is a necessary, but not sufficient, condition for stable points.*

Proof. The rate of change of the purity is

$$\dot{P}(\rho) = 2\text{Tr}(\rho\dot{\rho}) = 2\text{Tr}[\rho\mathcal{L}_D(\rho)], \quad (14)$$

or, equivalently, $P(\mathbf{v}) = \frac{1}{d} + \|\mathbf{v}\|^2$ and

$$\dot{P} = 2\mathbf{v} \cdot \dot{\mathbf{v}} = 2\mathbf{v} \cdot (R\mathbf{v} + \mathbf{c}). \quad (15)$$

Note that \dot{P} is independent of the control Hamiltonian, since $\text{Tr}(\rho[H, \rho]) = 0$. Consider a coherence vector $\mathbf{v} \in \mathbb{R}^{d^2-1}$, with a corresponding $d \times d$ -dimensional density matrix ρ . For a stable point, $\dot{\mathbf{v}} = 0$; therefore $\dot{P} = 2\mathbf{v} \cdot \dot{\mathbf{v}} = 0$, which proves necessity. For insufficiency, note first that \mathbf{v} has a $d^2 - 2$ dimensional orthogonal space. Following the same argument as in Proposition 2, we can diagonalize the density matrix as $\rho = \sum_{j=0}^{d-1} \beta_j |\beta_j\rangle\langle\beta_j|$ and write H in the same basis as $H = \sum_{k,l=0}^{d-1} h_{kl} |\beta_k\rangle\langle\beta_l|$, so that $-i[H, \rho] = -i \sum_{k \neq l} h_{kl} (\beta_l - \beta_k) |\beta_k\rangle\langle\beta_l|$. Thus, $-i[H, \rho]$ belongs to an orthogonal subspace of dimension at most $d^2 - d < d^2 - 2$ when $d > 2$. Therefore there exist states ρ and dissipators \mathcal{L}_D for which no H can found such that $-i[H, \rho] + \mathcal{L}_D \rho = 0$. \square

We show later (Proposition 7) that in the qubit case ($d = 2$), $\dot{P} = 0$ is also a sufficient condition for stable points.

Note that stable points are inherent to the dissipator, not the target property. The definition of stable points along with Eq. (1a) implies that there exists a Hamiltonian H such that $\mathcal{L}(\rho) = \mathcal{L}_H(\rho) + \mathcal{L}_D(\rho) = 0$. The following proposition builds on this and further characterizes stable points:

Proposition 4. *A system state is stable if it satisfies $\Pi_\lambda \mathcal{L}_D(\rho) \Pi_\lambda = 0$ for every eigenspace projector Π_λ of ρ .*

The proof needs the following ingredients and lemma: Given a Hermitian matrix B with eigenspace projectors $\{\Pi_l\}$, define the set $\mathcal{E}_B \equiv \{A = -i[H, B] : H = H^\dagger\}$ and $\mathcal{E}'_B \equiv \{A : \Pi_l A \Pi_l = 0 \forall \Pi_l\}$.

Lemma 1. $A \in \mathcal{E}_B \iff A \in \mathcal{E}'_B$.

This lemma can be viewed as characterizing the action of the Hamiltonian (H) as inducing a zero instantaneous change in the eigenspace of the density matrix (B).

Proof. Assume that $A \in \mathcal{E}_B$. Then $A = \mathcal{L}_H(B) = -i[H, B]$ for some Hamiltonian H . The spectral decomposition of B is $\sum_{j=1}^d \lambda_j \Pi_j$, and H can be written in the same basis as $\sum_{j,k=1}^d h_{jk} |\lambda_j\rangle\langle\lambda_k|$, where $\Pi_j |\lambda_k\rangle = \delta_{\lambda_j \lambda_k} |\lambda_k\rangle$. Expanding the commutator yields:

$$A = -i[H, B] = -i \sum_{j,k=1}^d h_{jk} (\lambda_k - \lambda_j) |\lambda_j\rangle\langle\lambda_k|, \quad (16)$$

so that for every eigenspace projector Π_l of B :

$$\Pi_l A \Pi_l = -i \sum_{j,k=1}^d h_{jk} (\lambda_k - \lambda_j) \Pi_l \delta_{\lambda_l \lambda_j} \delta_{\lambda_k \lambda_l} = 0, \quad (17)$$

so $A \in \mathcal{E}'_B$.

Now assume that $A \in \mathcal{E}'_B$. Then $\Pi_l A \Pi_l = 0$ for all eigenspace projectors Π_l of B . Consequently, A can be expanded in the eigenbasis of B as $\sum_{k,l} a_{kl} |\lambda_k\rangle\langle\lambda_l|$ such that $a_{kl} = 0$ whenever $\lambda_k = \lambda_l$. The Hamiltonian H given by $\sum_{j,k} h_{jk} |\lambda_j\rangle\langle\lambda_k|$ where

$$h_{jk} = \begin{cases} -i \frac{a_{jk}}{\lambda_j - \lambda_k} & \text{if } \lambda_j \neq \lambda_k \\ 0 & \text{otherwise} \end{cases}, \quad (18)$$

satisfies the relation $A = -i[H, B]$, which can be verified using Eq. (16). Therefore $A \in \mathcal{E}_B$. \square

We are now ready to prove Proposition 4.

Proof. If $\Pi_\lambda \mathcal{L}_D(\rho) \Pi_\lambda = 0$ for every eigenspace projector Π_λ of ρ , then by Lemma 1, $\mathcal{L}_D(\rho)$ can be written as $-i[H', \rho]$ for some Hermitian matrix H' . We can set the Hamiltonian to be $-H'$, leading to $\dot{\rho} = 0$ in Eq. (1), thus preserving that state and by extension, any target property. \square

Assuming that stable points exist for a given dissipator, the ultimate goal of the quantum tracking control protocol could be seen as *guiding the system from a given initial state to a stable point*, if possible. The reason is self-evident: reaching a stable point guarantees that the target property will be preserved. However, the stable point might not be reachable from a given initial state by applying a finite control Hamiltonian. We discuss this in detail next.

G. Breakdown points, f -preserving trajectories

At the opposite extreme of stable points are singularities of the control Hamiltonian associated with uncontrollable target properties. We call such singularities *breakdown points*; they are points at which an f -preserving control Hamiltonian [Eq. (12)] diverges. More formally:

Definition 9. For a given target property f and dissipator \mathcal{L}_D , a state is called a breakdown point ρ_b if (a) $[\rho_b, \nabla f] = 0$ and (b) $\langle \nabla f, \mathcal{L}_D \rho_b \rangle \neq 0$. The breakdown time t_b is the evolution time to a breakdown point.

The first example of a breakdown point and time was identified in Ref. [50] in the context of a dephasing Lindbladian (Example 1) with coherence as the target property. More generally, singularities are a well-known feature of tracking control [37–40].

Proposition 5. An f -preserving trajectory does not pass through breakdown points.

Proof. Suppose ρ is a breakdown point on the f -preserving trajectory. By definition, $i[\rho, \nabla f] = 0$. But from Eq. (11), this means $\langle \nabla f, \mathcal{L}_D \rho_b \rangle = 0$, which contradicts our assumption. \square

Next, we argue that the set of breakdown points introduces holes or partitions in the f level set hypersurface. This hypersurface is a geometric object in $\mathcal{M}^{(d)}$, the convex set of coherence vectors mentioned in Section II A. The control Hamiltonian can preserve the target property within each such partition but not between different partitions. To formalize this, let the level set of f be represented by the surface $S_f \in \mathcal{M}^{(d)}$, let $\mathbb{B}_{f,D}$ be the set of breakdown points given f and \mathcal{L}_D (or D), and let $S'_f \equiv S_f \setminus \mathbb{B}_{f,D}$ (the level set minus the set of breakdown points).

Definition 10. Two states ρ_a and ρ_b with respective coherence vector $\mathbf{v}_a \in S_f$ and $\mathbf{v}_b \in S_f$ are disconnected if for all differentiable trajectories $\mathbf{l}: [0, 1] \mapsto \mathcal{M}^{(d)}$ with beginning and end points $\mathbf{l}(0) = \mathbf{v}_a$ and $\mathbf{l}(1) = \mathbf{v}_b$, there exists $u \in (0, 1)$ s.t. $\mathbf{l}(u) \notin S'_f$.

In other words, every trajectory must pass through one or more breakdown points to connect the disconnected states ρ_a and ρ_b . The following clarifies what this means in terms of target-property-preserving trajectories:

Proposition 6. A system starting from a point in S'_f cannot reach a disconnected point in S'_f via an f -preserving trajectory.

Proof. Suppose an f -preserving trajectory does exist between two disconnected states ρ_a and ρ_b . Consider a state ρ' and corresponding coherence vector \mathbf{v}' on the portion of the trajectory lying outside S'_f . At this point, either $f(\rho') \neq f(\rho_a)$ (not on the level set) or $\mathbf{v}' \in \mathbb{B}_{f,D}$ (a breakdown point, i.e., the control Hamiltonian diverges). \square

An f -preserving trajectory can reach a stable point from an unstable point, but not always: there are cases where a stable point can only be reached from another stable point (see Section IV A 2).

H. Control-independent characterization of f -preserving trajectories

Suppose one wishes to steer a system from a given initial point ρ (e.g., an unstable point) to a final point σ (e.g., a stable point) while preserving the target f . From a Hamiltonian-first perspective, we choose a control Hamiltonian and evolve the state. However, this approach does not readily yield a Hamiltonian control and state trajectory compatible with the final state and the f -preservation constraint. Here, we address an alternative way of approaching the problem: we choose a trajectory instead of a Hamiltonian and determine whether such a given trajectory between two such given points is realizable, as defined in Section II B.

1. *A control-independent characterization of realizable trajectories*

The system's evolution is captured by two different processes in Eq. (1a): \mathcal{L}_H , which generates unitary dynamics, and \mathcal{L}_D , which generates non-unitary dynamics. This implies that the dissipation-adjusted system evolution is unitary: $\dot{\rho}(t) - \mathcal{L}_D\rho(t) = \mathcal{L}_H\rho(t)$. It turns out that the set of all trajectories generated by varying Hamiltonians can be characterized by this insight via Lemma 1. We formalize this next.

Consider a parametrized trajectory $\mathbf{I} : [0, 1] \rightarrow \mathcal{M}^{(d)}$. This corresponds to an operator-valued trajectory $\sigma : [0, 1] \rightarrow \mathcal{B}_+(\mathcal{H})$ using the nice operator basis. Let $\{\lambda_i\}$ and $\{\Pi_i\}$ represent the eigenvalues and corresponding eigenprojectors of a Hermitian operator. Recall that a realizable trajectory is a solution of Eq. (1) for some Hamiltonian H , or, equivalently, Eq. (2) for some Q .

Lemma 2. *Let $\sigma(u) = \sum_i \lambda_i(u)\Pi_i(u)$ be the spectral decomposition of $\sigma(u)$. Then, the corresponding trajectory $\mathbf{I}(u)$ is equivalent to a realizable trajectory iff $\forall \Pi_i(u), u \in [0, 1]$:*

$$\Pi_i(u)[\partial_u\sigma(u) - c(u)\mathcal{L}_D\sigma(u)]\Pi_i(u) = 0, \quad (19)$$

for some $c(u)$ where $0 < c(u) < \infty$.

Proof. \implies : Since, by assumption, Eq. (19) holds for all eigenspace projectors $\Pi_i(u)$, by Lemma 1 there exists a Hermitian operator $H(u)$ such that:

$$\partial_u\sigma(u) - c(u)\mathcal{L}_D\sigma(u) = -i[H(u), \sigma(u)]. \quad (20)$$

At this point, it is already clear that $\sigma(u)$ represents a solution of Eq. (1) for some Hamiltonian, and therefore corresponds to a realizable trajectory. However, some extra work is required to account for the parametrization.

Reparameterizing with $dt = c(u)du$ yields a transform from the interval $I_1 = [0, 1]$ to a new interval $I_2 = [0, \varphi(1)]$ where $\varphi(s) = \int_0^s c(u)du$. Since $c(u)$ is positive, the inverse transform $M^{-1} : I_2 \rightarrow I_1$ is also well defined. Defining $\rho(t) \equiv \sigma(\varphi^{-1}(t))$ and $H_0(t) \equiv \frac{1}{c(\varphi^{-1}(t))}H(\varphi^{-1}(t))$ for $t \in I_2$, Eq. (20) becomes

$$\dot{\rho}(t) = -i[H_0(t), \rho(t)] + \mathcal{L}_D\rho(t). \quad (21)$$

Since $c(u)$ is finite and non-zero $\forall u \in I_1$, it follows that $H_0(t)$ is finite $\forall t \in I_2$. Moreover, if the nice operator basis representation of $\rho(t)$ is $\mathbf{v}(t)$, then $\mathbf{v}(t) = \mathbf{v}(\varphi(u)) = \mathbf{I}(u)$ where φ is continuously differentiable, and $\partial_u\varphi(u) > 0$. Therefore, by Definition 1, $\mathbf{I}(u)$ is equivalent to the realizable trajectory $\mathbf{v}(t)$.

\impliedby : Suppose $\mathbf{I} : [0, 1] \mapsto \mathcal{M}^{(d)}$ is equivalent to a realizable trajectory $\mathbf{v} : [0, t_f] \mapsto \mathcal{M}^{(d)}$, which corresponds to a density operator evolution given by $\rho(t)$. Then, by Definition 1, $\mathbf{I}(u) = \mathbf{v}(\varphi(u))$ for some continuously differentiable map $\varphi : [0, 1] \mapsto [0, t_f]$. In the nice operator basis, this corresponds to $\sigma(u) = \rho(\varphi(u))$ where σ is the

representation of \mathbf{I} in the operator space. Since \mathbf{v} is realizable

$$\dot{\rho}(t) = -i[H(t), \rho(t)] + \mathcal{L}_D\rho(t). \quad (22)$$

for some $H(t)$. Substituting $t = \varphi(u)$ gives

$$\frac{1}{\partial_u\varphi(u)}\partial_u\sigma(u) = -i[H(\varphi(u)), \sigma(u)] + \mathcal{L}_D\sigma(u), \quad (23)$$

which implies

$$\partial_u\sigma(u) - \partial_u\varphi(u)\mathcal{L}_D\sigma(u) = -i[\partial_u\varphi(u)H(\varphi(u)), \sigma(u)], \quad (24)$$

where $\partial_u\varphi(u) > 0$. Finally, applying Lemma 1 gives the required result. \square

Once we have a realizable trajectory, we can find the control Hamiltonian which realizes it:

Theorem 2. *Let $\sigma(u), c(u)$ be as in Lemma 2. Then the actual realizable trajectory is given by the state $\rho(t) = \sigma(\varphi^{-1}(t))$ where $\varphi(s) = \int_0^s c(u)du$.*

Moreover, a control Hamiltonian which realizes this trajectory is

$$H(t) = \sum_{j,k} h_{jk}(t)|\lambda_j(t)\rangle\langle\lambda_k(t)| \quad (25a)$$

$$h_{jk} = -i \frac{\langle\lambda_j|\dot{\rho} - \mathcal{L}_D\rho|\lambda_k\rangle}{\lambda_j - \lambda_k}, \quad (25b)$$

where $\{\lambda_j(t)\}, \{|\lambda_j(t)\rangle\}$ denote the eigenvalues and eigenvectors of $\rho(t)$ respectively.

Proof. $\rho(t) = \sigma(\varphi^{-1}(t))$ follows from the proof of Lemma 2. Then, $\dot{\rho} = -i[H, \rho] + \mathcal{L}_D\rho$. Rearranging gives $-i[H, \rho] = \dot{\rho} - \mathcal{L}_D\rho$. The particular form of H follows from the proof of Lemma 1, specifically Eq. (18). \square

An example of designing the control Hamiltonian based on the trajectory is provided in Appendix D 1.

2. *Result for f -preserving trajectories*

The corollary below emphasizes that characterizing realizable f -preserving trajectories requires enforcing f -preservation in any one of the equivalent trajectories.

Corollary 1. *$f(\mathbf{I}(u))$ in Lemma 2 is constant over the trajectory iff $\mathbf{I}(u)$ is equivalent to a realizable f -preserving trajectory.*

Proof. \implies : By Lemma 2, $\mathbf{I}(u)$ is equivalent to a realizable trajectory $\mathbf{v}(t)$, where $\mathbf{v}(t) = \mathbf{I}(\varphi(u))$ for some continuously differentiable φ . Then $f(\mathbf{v}(t)) = f(\mathbf{I}(\varphi(u))) = \text{const}$. Therefore, $\mathbf{v}(t)$ is an f -preserving trajectory.

\impliedby : $\mathbf{I}(u)$ is equivalent to a realizable trajectory, $\mathbf{v}(t)$ where $\mathbf{v}(\varphi(t)) = \mathbf{I}(u)$ for some continuously differentiable φ . By assumption, $f(\mathbf{v}(t)) = \text{const}$. Therefore $f(\mathbf{I}(u)) = f(\mathbf{v}(\varphi(t))) = \text{const}$. \square

This answers the question that motivated this subsection of how to steer a system from a given initial point ρ (e.g., an unstable point) to a final point σ (e.g., a stable point) while preserving the target f : we choose potential trajectories and check whether they are realizable trajectories. Crucially, the check can be done without knowing the control Hamiltonian due to Lemma 2. Once a realizable trajectory is found, the control Hamiltonian can be found using Theorem 2.

III. THE SINGLE-QUBIT CASE: GENERAL THEORY

We now specialize to the single-qubit case to gain intuition and illustrate the general theory. Due to the simplicity of the Bloch sphere picture, we present our results in this section using the Bloch vector formalism. Thus, we now consider differentiable trajectories $\mathbf{l} : [0, 1] \mapsto S^2$, the unit sphere in \mathbb{R}^3 .

A. Qubit tracking control

Both the Hamiltonian and the density matrix can be expanded in the (unnormalized) Pauli basis: $H = h_0 I + \mathbf{h} \cdot \boldsymbol{\sigma}$ with $\mathbf{h} = (h_x, h_y, h_z) \in \mathbb{R}^3$, and $\rho = \frac{1}{2}(I + \mathbf{v} \cdot \boldsymbol{\sigma})$, where $\mathbf{v} \in S^2$ (the unit sphere in \mathbb{R}^3) is now the Bloch vector, as opposed to the coherence vector.¹ In this case, the unitary dynamics component in Eq. (2) is given by $Q\mathbf{v} = 2\mathbf{h} \times \mathbf{v}$, where \times denotes the cross product in \mathbb{R}^3 (see Appendix B). We tabulate the dissipators $D = (R, \mathbf{c})$ for various noise channels in Appendix B.

Therefore, the dynamics [Eq. (2)] and constraint [Eq. (6b)] equations that govern the tracking control problem in the single-qubit case are, respectively:

$$\dot{\mathbf{v}} = 2\mathbf{h} \times \mathbf{v} + R\mathbf{v} + \mathbf{c} \quad (26a)$$

$$\nabla f \cdot (2\mathbf{h} \times \mathbf{v} + R\mathbf{v} + \mathbf{c}) = 0, \quad (26b)$$

where in the tracking control problem $\mathbf{h} = \mathbf{h}(\mathbf{v})$.

Note that the cross product is the specialization of the commutator (over the vector space of Hermitian matrices) to \mathbb{R}^3 : they share the standard properties of bilinearity, anticommutativity, and the Jacobi identity. Moreover, $[A, B]$ is likewise orthogonal to both A and B , i.e., $\langle A, [A, B] \rangle = \langle B, [A, B] \rangle = 0$, and both satisfy the cyclic property $\langle A, [B, C] \rangle = \langle C, [A, B] \rangle$. Finally, the cross-product vanishes when both the input vectors are collinear, similar to the commutator (which vanishes if the operators share the same eigenspace, i.e., if they are diagonal in the same basis).

¹ The Bloch vector and the coherence vector differ by normalization, since the latter is defined via $\rho = \frac{1}{2}I + \mathbf{v} \cdot \boldsymbol{\sigma}$.

B. Uncontrollable target properties

Using Eq. (9) and $Q\mathbf{v} = 2\mathbf{h} \times \mathbf{v}$, uncontrollable target properties are characterized by:

$$\nabla f \cdot (\mathbf{h}(\mathbf{v}) \times \mathbf{v}) = \mathbf{h}(\mathbf{v}) \cdot (\mathbf{v} \times \nabla f) = 0. \quad (27)$$

For a given Bloch vector \mathbf{v} , this condition holds if $\mathbf{h}(\mathbf{v})$ is orthogonal to $\nabla f \times \mathbf{v}$, and for all control Hamiltonians \mathbf{h} iff $\nabla f \propto \mathbf{v}$.

For a qubit (but not in higher-dimensional Hilbert spaces), Proposition 1 rules out the preservation of any target property which is purely a function of the eigenvalues of the density matrix, since these are given by $\lambda_{1,2} = \frac{1}{2}(1 \pm v)$ (see Appendix B). This includes the set of Rényi α -entropies: $f(\mathbf{v}) = \frac{1}{1-\alpha} \ln(\lambda_1^\alpha + \lambda_2^\alpha)$, which reduces to the von Neumann entropy $-\lambda_1 \ln(\lambda_1) - \lambda_2 \ln(\lambda_2)$ for $\alpha \rightarrow 1$.

C. Stable point loci

Stable points are Bloch vectors for which $\mathbf{h}(\mathbf{v})$ can be chosen so that $\dot{\mathbf{v}} = 0 \forall t$ (Definition 7). In the qubit case, the purity $P(\mathbf{v}) = \frac{1}{2}(1 + \|\mathbf{v}\|^2)$ and

$$\dot{P} = \mathbf{v} \cdot \dot{\mathbf{v}} = \mathbf{v} \cdot (R\mathbf{v} + \mathbf{c}). \quad (28)$$

We now specialize Proposition 3 to the qubit case, showing that $\dot{P} = 0$ is necessary and sufficient for stable points.

Proposition 7. *In the single-qubit case, the locus of stable points is independent of the control Hamiltonian and is characterized by a constant purity, i.e., it satisfies*

$$\dot{P} = 0. \quad (29)$$

Conversely, the unstable points are characterized by $\dot{P} \neq 0$.

Proof. Eq. (28) is independent of the control Hamiltonian \mathbf{h} , since $\mathbf{v} \cdot \mathbf{h} \times \mathbf{v} = 0$. If $\mathbf{v} \cdot (R\mathbf{v} + \mathbf{c}) = 0$, then $R\mathbf{v} + \mathbf{c}$ is orthogonal to \mathbf{v} (or a zero vector) and hence can be written as $2\mathbf{h}' \times \mathbf{v}$ for some vector \mathbf{h}' . We can set the Hamiltonian to be $-\mathbf{h}'$, which leads to $\dot{\mathbf{v}} = 0$, and the point is stable. Conversely, if $\dot{P} \neq 0$, then using Eq. (28) we have $\mathbf{v} \cdot \dot{\mathbf{v}} \neq 0$, i.e., $\dot{\mathbf{v}} \neq 0$. Therefore, the point is unstable. \square

Example 3: Consider Example 1 again. The stable points are given by Eq. (29), which yields $\mathbf{v} \cdot (R\mathbf{v} + \mathbf{c}) = \mathbf{v} \cdot \text{diag}(-2\gamma, -2\gamma, 0)\mathbf{v} = -2\gamma(v_x^2 + v_y^2) = 0$, i.e., the z -axis. Points off the z -axis are unstable.

We proceed to give a geometric characterization of the stable point loci. As mentioned above, when working in a nice operator basis, R in Eq. (1) is a symmetric matrix in the single qubit case. We can then diagonalize R via an orthogonal matrix O : $R = ODO^T$ where

$D = -\text{diag}(d_1, d_2, d_3)$ is a negative semi-definite diagonal matrix of R 's eigenvalues (some but not all of the eigenvalues can be zero), and O 's columns are R 's corresponding eigenvectors. The dissipator can then be rewritten as:

$$R\mathbf{v} + \mathbf{c} = O(D\mathbf{w} + \mathbf{c}')O^T. \quad (30)$$

where $\mathbf{w} = O^T\mathbf{v}O$, $\mathbf{c}' = O^T\mathbf{c}O$. Note that the vector \mathbf{c}' is constrained to be in the column space of D . Eq. (29) then implies that the locus of stable points satisfies $\mathbf{v}^T(R\mathbf{v} + \mathbf{c}) = O\mathbf{w}^T(D\mathbf{w} + \mathbf{c}')O^T = 0$, i.e., the quadratic form

$$\sum_{i=1}^3 d_i(w_i - r_i)^2 = r^2, \quad r_i = \frac{1}{2} \frac{c'_i}{d_i}, \quad (31)$$

where $r = \|\mathbf{r}\|$, $\mathbf{r} = (r_1, r_2, r_3)$, and the notation \sum' indicates that if $d_i = 0$ then the corresponding term is absent in the sum.

1. Unital channels

For unital channels, $\mathbf{c} = \mathbf{0}$, which reduces Eq. (31) to $\sum_{i=1}^3 d_i w_i^2 = 0$, which means that the locus of stable points is limited to:

1. The origin: $r = 0$ and all $d_i > 0$, or
2. A line: two of the $d_i > 0$ and the line is along the axis corresponding to the zero d_i , or
3. A plane: two of the d_i are zero, and the plane is through the origin, orthogonal to the axis corresponding to the nonzero d_i .

2. Non-unital channels

For non-unital channels, where $\mathbf{c} \neq \mathbf{0}$, Eq. (31) describes:

1. An ellipsoid centered at \mathbf{r} : all $d_i > 0$.
2. An elliptic cylinder: two of the $d_i > 0$, the cylinder extends along the axis corresponding to the zero d_i .
3. Two parallel planes: e.g., $d_2 = d_3 = 0$ and the two planes are through the origin and through $w_1 = 2r$, orthogonal to the axis corresponding to $d_1 \neq 0$.

Below, we give examples of all these different cases using various noise channels.

D. Stable points and purity preservation

Stable points are related to purity preservation in the single-qubit case:

Proposition 8. *If there exist two times $t_1 < t_2$ such that the purity $P(t_1) = P(t_2)$, then the system must pass through a stable point $t' \in (t_1, t_2)$.*

Proof. The purity of a qubit is given by $P(t) = \frac{1}{2}[1 + v^2(t)]$, where $v = \|\mathbf{v}\|$. Since $P(t_1) = P(t_2)$, then by Rolle's theorem there exists a time $t' \in (t_1, t_2)$ such that

$$0 = \dot{P}(t)|_{t'}. \quad (32)$$

The last equality represents a stable point. \square

Thus, any *periodic* Bloch vector trajectory passes through a stable point. Note that this result does not generalize to higher-dimensional spaces since it relies on Proposition 7.

E. f -preserving Hamiltonians and breakdown points

Using the Bloch vector formalism, it is instructive to specialize Theorem 1 to the single-qubit case.

Corollary 2. *For any controllable target property of a qubit, the f -preserving component of the tracking control Hamiltonian may always be written as*

$$\mathbf{h} = \frac{\nabla f \cdot (R\mathbf{v} + \mathbf{c})}{2\|\nabla f \times \mathbf{v}\|^2} \nabla f \times \mathbf{v}. \quad (33)$$

Proof. This follows immediately from Eq. (12) upon replacing $\mathcal{L}_D\rho$ with $R\mathbf{v} + \mathbf{c}$ [Eq. (2)], $i[\rho, \nabla f]$ with $\nabla f \times \mathbf{v}$ (i.e., the commutator with the vector product, as argued above), and the coherence vector by the Bloch vector. The factor of 2 is an artifact of using $\boldsymbol{\sigma}$ as a basis for \mathbf{h} instead of $\boldsymbol{\sigma}/2$. \square

We present an alternative proof that does not rely on Eq. (12). This proof has the advantage of exposing the components of \mathbf{h} that play no role in f -preservation but are crucial in extending the breakdown time, as will be shown later.

Proof. It follows from Eq. (27) that to avoid the uncontrollable case, \mathbf{v} and ∇f must be linearly independent vectors. Therefore the set $\{\mathbf{v}, \nabla f, \nabla f \times \mathbf{v}\}$ forms a basis for \mathbb{R}^3 . Expanding \mathbf{h} in this basis as

$$\mathbf{h} = \alpha_1\mathbf{v} + \alpha_2\nabla f + \alpha_3\nabla f \times \mathbf{v}, \quad (34)$$

and substituting into Eq. (26b), we obtain:

$$\nabla f \cdot (2(\alpha_1\mathbf{v} + \alpha_2\nabla f + \alpha_3\nabla f \times \mathbf{v}) \times \mathbf{v} + R\mathbf{v} + \mathbf{c}) = 0. \quad (35)$$

The terms involving α_1 and α_2 vanish, while $\nabla f \cdot [(\nabla f \times \mathbf{v}) \times \mathbf{v}] = -\|\nabla f \times \mathbf{v}\|^2$, which implies:

$$\alpha_3 = \frac{1}{2} \frac{\nabla f \cdot (R\mathbf{v} + \mathbf{c})}{\|\nabla f \times \mathbf{v}\|^2}. \quad (36)$$

The other two terms in Eq. (34) vanish in the constraint equation [Eq. (26b)], so they play no role in preserving f . Therefore the f -preserving component of \mathbf{h} is $\alpha_3 \nabla f \times \mathbf{v}$. \square

Corollary 2 is consistent with our analysis of uncontrollable target properties in Section IID 2, since if $\nabla f \propto \mathbf{v}$, then $\mathbf{h} \rightarrow \infty$ in Eq. (33). This also motivates specializing the definition of breakdown points (Definition 9) to the qubit case:

Definition 11. For a given target property f and dissipator D , we call a Bloch vector a breakdown point \mathbf{v}_b if (a) $\nabla f|_{\mathbf{v}_b} \propto \mathbf{v}_b$ and (b) $\dot{P}(\mathbf{v}_b) \neq 0$ (i.e., \mathbf{v}_b is unstable).

Thus, a breakdown point is a point where \mathbf{h} [Eq. (33)] diverges. As before, the breakdown time t_b is the time when the state reaches a breakdown point.

In the context of Example 1, the breakdown condition $\nabla f|_{\mathbf{v}_b} \propto \mathbf{v}_b$ yields the entire (x, y) plane, but note that the condition $\dot{P}(\mathbf{v}_b) \neq 0$ excludes the origin. We find the breakdown time below, in Section IV A 2.

Note that Corollary 2 fixes the component of \mathbf{h} in the $\nabla f \times \mathbf{v}$ direction. In practice, keeping components along the directions ∇f and \mathbf{v} non-zero may be advantageous, in case this simplifies the implementation of the control Hamiltonian. Moreover, the component along ∇f can also affect the breakdown time (e.g., see Section IV A 3).

The reason that only one component of \mathbf{h} appears in Eq. (33) has a simple geometric interpretation: the component of \mathbf{h} along \mathbf{v} has no effect, while the ∇f component moves the state *along* f 's level set. Counteracting the dissipator requires \mathbf{h} 's component $\mathbf{v} \times \nabla f$ since both it and the dissipator move \mathbf{v} *away* from f 's level set.

F. Realizable trajectories

Let $\mathbf{l} : [0, 1] \mapsto S^2$ denote an arbitrary parameterized Bloch sphere trajectory that is not necessarily a solution of the master equation [Eq. (26a)].

Definition 12. The trajectory purity is

$$P[\mathbf{l}(u)] = \frac{1}{2}[1 + \|\mathbf{l}(u)\|^2]. \quad (37)$$

The dissipator-induced purity rate is

$$\partial_u P_D[\mathbf{l}(u)] \equiv \mathbf{l}(u) \cdot (R\mathbf{l}(u) + \mathbf{c}). \quad (38)$$

The former is the formal purity associated with the trajectory $\mathbf{l}(u)$. The latter can be interpreted as the rate of purity change due to the dissipator $D = (R, \mathbf{c})$ for the trajectory $\mathbf{l}(u)$. We emphasize that this purity rate is not necessarily related to the solution of the master equation either.

From Eq. (28), if \mathbf{l} were equivalent (in the sense of Definition 1) to a solution of Eq. (26a), then $\partial_u P_D = \partial_u P$. Conversely, is a trajectory that satisfies $\partial_u P_D \propto \partial_u P$ always realizable? The following result resolves this question:

Proposition 9. $\mathbf{l}(u)$ is equivalent to a realizable trajectory iff

$$\partial_u P[\mathbf{l}(u)] = c(u) \partial_u P_D[\mathbf{l}(u)], \quad (39)$$

where $0 < c(u) < \infty \forall u \in [0, 1]$.

Proof. From Lemma 2, if the Bloch vector trajectory $\mathbf{l}(u)$ corresponds to a density matrix trajectory $\sigma(u)$, then Eq. (19) is satisfied iff $\mathbf{l}(u)$ (which is the same as the coherence vector up to a scalar multiplicative factor) is equivalent to a realizable trajectory. Eq. (20) can be written as

$$\partial_u \mathbf{l}(u) - c(u)[R\mathbf{l}(u) + \mathbf{c}] = 2\mathbf{h} \times \mathbf{l}(u). \quad (40)$$

In \mathbb{R}^3 , orthogonal directions are uniquely determined by the cross product, i.e., if $\mathbf{a}, \mathbf{b} \in \mathbb{R}^3$, $\mathbf{a} \cdot \mathbf{b} = 0 \iff \mathbf{a} = \mathbf{b} \times \mathbf{c}$ for some non-zero $\mathbf{c} \in \mathbb{R}^3$. Thus, Eq. (40) holds iff

$$\mathbf{l}(u) \cdot [\partial_u \mathbf{l}(u) - c(u)(R\mathbf{l}(u) + \mathbf{c})] = 0, \quad (41)$$

which is Eq. (39). Since u was arbitrary, the statement must be true for all u . \square

IV. THE SINGLE-QUBIT CASE: EXAMPLES

In this section, we discuss several examples to illustrate the general theory. Table I gives the values of the control Hamiltonian [Eq. (33), all other components of \mathbf{h} set to 0] for two target properties: the square of the coherence magnitude

$$f = [\text{Tr}(\rho\sigma^x)]^2 + [\text{Tr}(\rho\sigma^y)]^2 = v_x^2 + v_y^2, \quad (42)$$

and the Uhlmann fidelity between two states ρ and σ :

$$f = \text{Tr}(\sqrt{\sqrt{\sigma}\rho\sqrt{\sigma}}), \quad (43)$$

See Appendix D for the derivation of most of the results in Table I. Fig. 1 illustrates the geometry of the Bloch sphere for three different noise channels and the two target properties above in terms of level sets, stable points, and breakdown points.

In the following, we use the shorthand “trajectory \mathbf{l} can be realized” to mean that trajectory \mathbf{l} is equivalent to a realizable trajectory.

A. Coherence

We first focus on the square of the coherence magnitude, which we refer to as the “coherence” for simplicity, and whose target constant value we denote by f_0 . Coherence is the experimental signature of the superposition structure (in a given basis) of quantum systems, which is one of the fundamental attributes of quantum mechanics [51]. Preserving coherence is, therefore, a task of fundamental interest, and the coherence-generating power of quantum operations has been studied extensively [52].

Target property → Noise channel ↓	Coherence magnitude $f = v_x^2 + v_y^2$	Uhlmann Fidelity $f = \text{Tr}(\sqrt{\sqrt{\sigma}\rho\sqrt{\sigma}})$
dephasing (Z)	$-\frac{\gamma}{v_z}(v_y, -v_x, 0)$	$\gamma[(k_0\mathbf{v} - \mathbf{w}) \cdot (v_x, v_y, 0)] \frac{\mathbf{w} \times \mathbf{v}}{\ \mathbf{w} \times \mathbf{v}\ ^2}$
bit-flip (X)	$\frac{-\gamma v_z^2}{v_z f}(v_y, -v_x, 0)$	$\gamma[(k_0\mathbf{v} - \mathbf{w}) \cdot (0, v_y, v_z)] \frac{\mathbf{w} \times \mathbf{v}}{\ \mathbf{w} \times \mathbf{v}\ ^2}$
bit-phase-flip (Y)	$\frac{-\gamma v_x^2}{v_z f}(v_y, -v_x, 0)$	$\gamma[(k_0\mathbf{v} - \mathbf{w}) \cdot (v_x, 0, v_z)] \frac{\mathbf{w} \times \mathbf{v}}{\ \mathbf{w} \times \mathbf{v}\ ^2}$
depolarizing	$\frac{-2\gamma}{3v_z}(v_y, -v_x, 0)$	$\frac{2}{3}\gamma[(k_0\mathbf{v} - \mathbf{w}) \cdot \mathbf{v}] \frac{\mathbf{w} \times \mathbf{v}}{\ \mathbf{w} \times \mathbf{v}\ ^2}$
relaxation at temperature T	$\frac{-\gamma}{4v_z}(v_y, -v_x, 0)$	$\frac{1}{4}\gamma[(k_0\mathbf{v} - \mathbf{w}) \cdot (v_x, v_y, 2(v_z - 2a))] \frac{\mathbf{w} \times \mathbf{v}}{\ \mathbf{w} \times \mathbf{v}\ ^2}$
relaxation at temperature T (γ_1) + dephasing (γ_d)	$\frac{-\gamma_2}{2v_z}(v_y, -v_x, 0)$	$\frac{1}{2}\gamma_2[(k_0\mathbf{v} - \mathbf{w}) \cdot (v_x, v_y, 2(v_z - 2a))] \frac{\mathbf{w} \times \mathbf{v}}{\ \mathbf{w} \times \mathbf{v}\ ^2}$

TABLE I. The control Hamiltonian [Eq. (33)] necessary to preserve two target properties (coherence and fidelity) for different environments. The system state ρ is represented by the Bloch vector $\mathbf{v} = (v_x, v_y, v_z)$ and σ by \mathbf{w} , $k_0 \equiv \frac{1 - \|\mathbf{w}\|^2}{1 - \|\mathbf{v}\|^2}$, $\gamma_2 \equiv 2\gamma_d + \frac{\gamma_1}{2}$ and $a \equiv [1 + \exp(-\beta\Delta)]^{-1} - 1/2$ where Δ is the qubit energy gap and $\beta = 1/T$ is the inverse temperature.

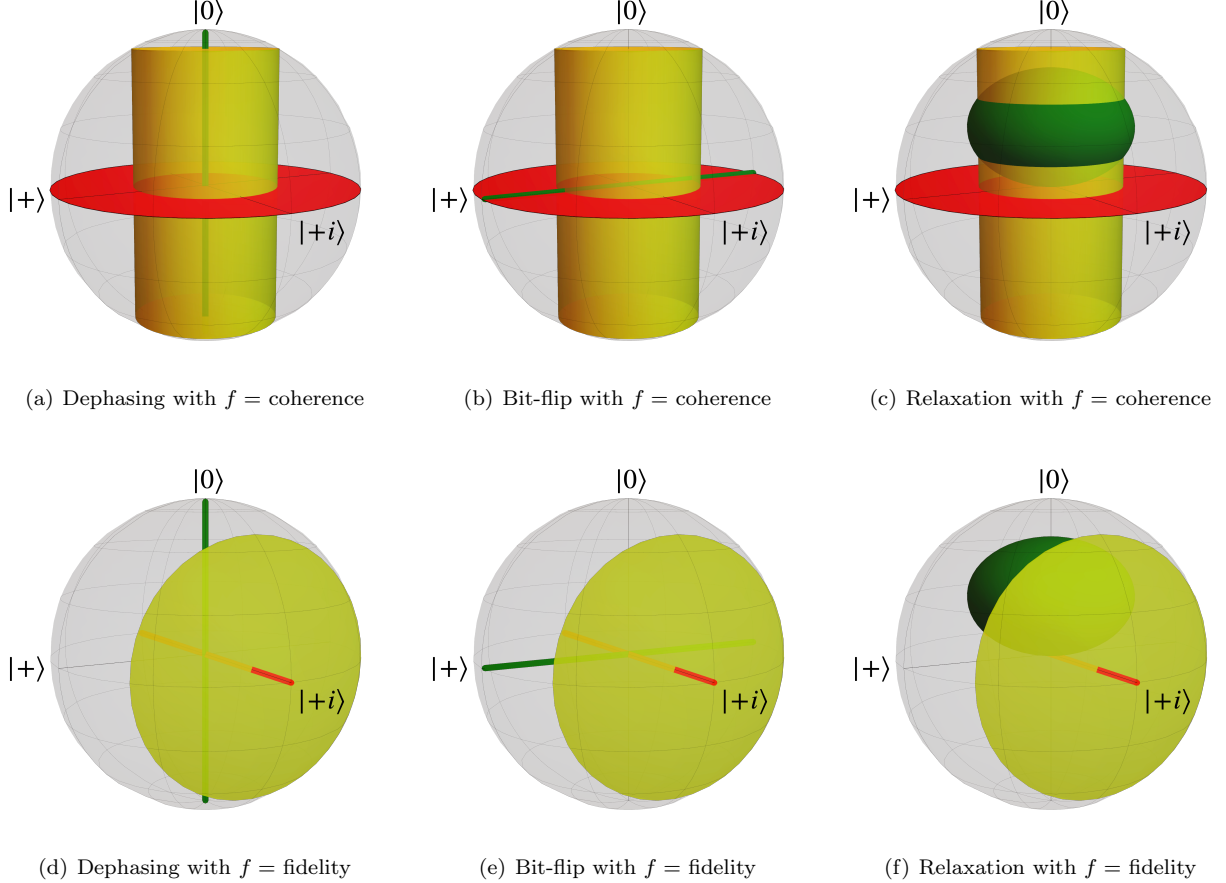


FIG. 1. Regions of level sets, stable points, and breakdown points for three different noise channels: dephasing (left column), bit-flip (middle column), and relaxation with $\beta\Delta = 2$ (right column). The target properties are the coherence magnitude (top row) and the fidelity with $|+i\rangle$ (bottom row). The grey spheres represent the Bloch sphere of a qubit. The stable region $[\mathbf{v} \cdot (R\mathbf{v} + \mathbf{c}) = 0]$ and breakdown region $(\nabla f \propto \mathbf{v})$ are indicated by green and red, respectively. The yellow regions represent the level sets for a given initial state with initial coherence $v_x^2 + v_y^2 = 0.22$ in panels (a)-(c) and initial fidelity 0.8 with $\mathbf{w} = (0, 1, 0)$ in panels (d)-(f).

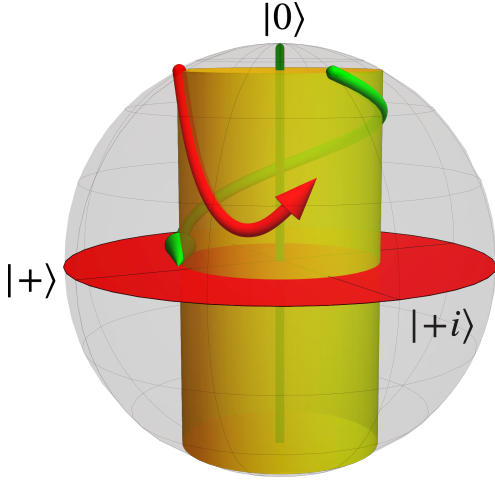


FIG. 2. Illustration of Proposition 9 for coherence preservation under dephasing (Example 1). The red trajectory has an increasing purity and, therefore, cannot be realized. The green trajectory has decreasing purity and terminates before the breakdown region. Since it satisfies all conditions of Proposition 9, it is realizable.

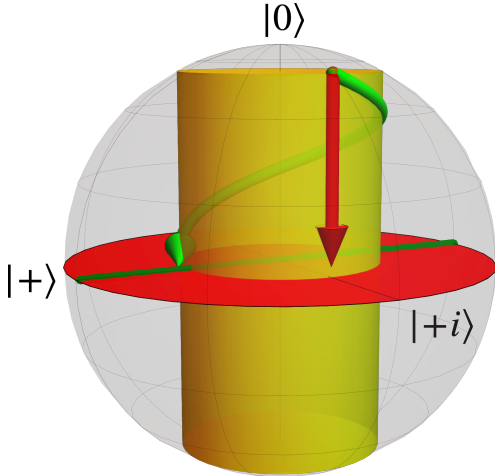


FIG. 3. Landscape of the Bloch sphere for the bit-flip channel, showing the cylindrical level set (yellow surface), the breakdown set in the (x, y) plane (red disk), the set of stable points along the x -axis (green line), and two trajectories: a coherence-preserving trajectory that travels along the level set towards the stable set (green arrow), and a trajectory with a breakdown point at its end (red arrow).

1. Level set and breakdown points

Note that the coherence evades the no-go result of Proposition 1: it does not depend only on $\|\mathbf{v}\|$. Indeed, for the coherence magnitude $f = f_0 = v_x^2(0) + v_y^2(0)$, we have $\nabla f = (2v_x, 2v_y, 0)$ and the level set is a cylinder of radius $\sqrt{f_0}$, whose axis is the z -axis, as illustrated by the cylinders in Fig. 1(a)-(c). It follows from Definition 11 that the set of breakdown points is the entire (x, y) plane except for the stable points in the plane. The role of the

control landscape will be more evident below, where we consider several noise models.

2. Dephasing

We revisit Example 1, for which the level set with non-zero coherence magnitude $f_0 = v_x^2(0) + v_y^2(0)$ forms a vertical cylinder. What are the realizable trajectories? As shown in Example 3, the unstable points are the points not on the z -axis. For any such point we have $\partial_u P_D(\mathbf{l}) = \mathbf{l} \cdot (R\mathbf{l} + \mathbf{c}) = -2\gamma(l_x^2 + l_y^2) < 0$ where γ is the dephasing rate. However, for stable points, $\partial_u P_D(\mathbf{l}) = \mathbf{l} \cdot (R\mathbf{l} + \mathbf{c}) = 0$ from Proposition 7 and Eq. (28). Thus, as a consequence of Proposition 9, a trajectory can be realized iff

1. For the portion of the trajectory not on the z -axis, the derivative of the trajectory purity is also negative (i.e., the trajectory purity decreases) and
2. For points on the z -axis on the trajectory, the derivative of the trajectory purity is zero.

\mathbf{l} is equivalent to an f -preserving trajectory iff \mathbf{l} satisfies the conditions above and lies on a level set of f . For coherence preservation with $f_0 > 0$, the level set contains no points on the z -axis. Therefore, by Propositions 5 and 9, any trajectory on the cylindrical level set which (i) has a decreasing purity and (ii) does not cross the breakdown region, i.e., the (x, y) plane, is realizable. An example is illustrated in Fig. 2: the purity of the red trajectory increases and, therefore, is not realizable. However, the green trajectory is realizable because it has a decreasing purity throughout and terminates before the breakdown region. For such a trajectory, after decreasing, $l_z(t)$ must eventually reach 0, i.e., the (x, y) plane, which is the region of breakdown points. The control Hamiltonian diverges at this point, and due to Proposition 6, it cannot reach a disconnected point.

Let us find the corresponding breakdown time. Using $v^2 = f_0 + v_z^2$, we obtain:

$$\partial_t(v_z^2) = \partial_t(v^2) = 2\dot{P}(\mathbf{v}) = -4\gamma f_0, \quad (44)$$

whose solution is $v_z^2(t) = v_z^2(0) - 4\gamma f_0 t$. Setting $v_z(t_b) = 0$ yields the breakdown time as

$$t_b = \frac{v_z^2(0)}{4\gamma f_0}, \quad (45)$$

which decreases, as might be expected, in inverse proportion to the dephasing rate γ and the initial coherence value f_0 . Note that t_b is independent of the Bloch vector trajectory; as will be evident in later examples, this is not a general result.

Conversely, an f -preserving trajectory can only reach a stable point if it starts at a stable point, i.e., if the trajectory is a point on the z -axis.

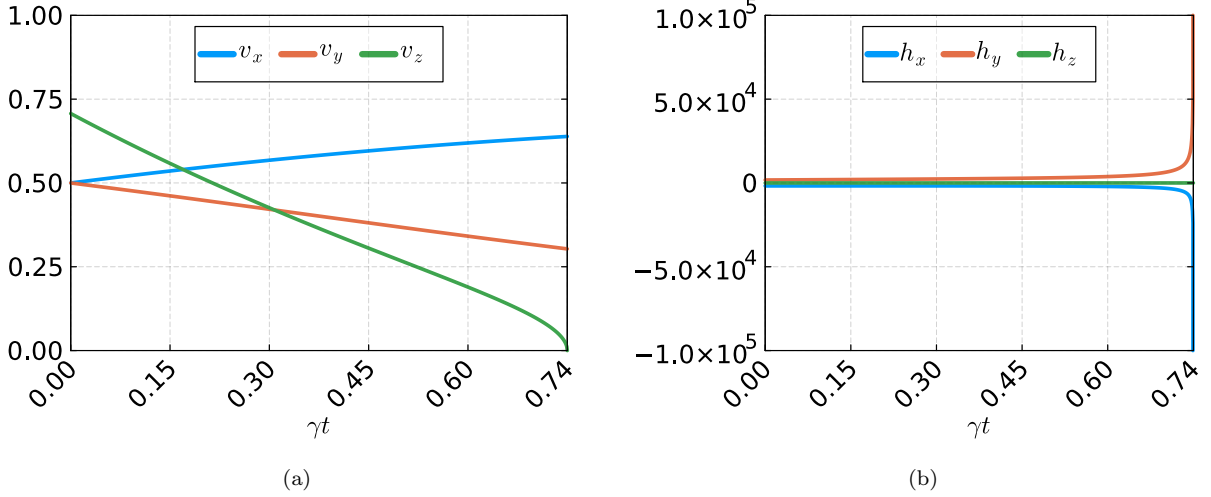


FIG. 4. Time dependence of the Bloch vector components (a) and the control Hamiltonian components (b) for preserving the coherence magnitude ($v_x^2 + v_y^2 = 0.5$) subject to the bit-flip channel, using only the necessary (α_3) component of the f -preserving Hamiltonian [Eq. (33)]. The initial state is $(1/2, 1/2, 1/\sqrt{2})$. Note that the Hamiltonian diverges near the breakdown point ($v_z = 0, v_x \neq 0$).

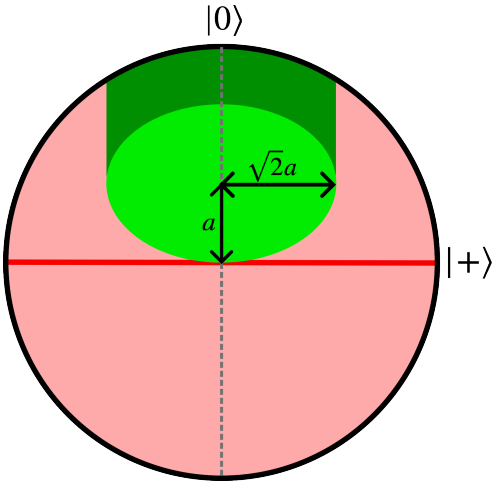


FIG. 5. Cross-sectional view ($v_y = 0$) of the initial state stability landscape for preserving coherence subject to pure relaxation ($a \equiv [1 + \exp(-\beta\Delta)]^{-1} - 1/2$). The purity decreases in the dark green area, while it increases inside the light green area. The two green areas combined are the initial states which lead to stable points. The other pink areas always lead to a breakdown point. The same structure applies when additional dephasing is present: the ellipsoid shrinks uniformly along the v_x and v_y axes. Note that $\mathbf{v} = (0, 0, 2a)$ is the steady state for relaxation.

3. Bit-flip

For the bit-flip channel, $L_\alpha = \sigma^x$ and the rate $\gamma_\alpha(t) = \gamma > 0$ in Eq. (1c). This corresponds to $R = \text{diag}(0, -2\gamma, -2\gamma)$ and $\mathbf{c} = \mathbf{0}$. The stable points [Eqs. (28) and (29)] are given by $\dot{P} = \mathbf{v} \cdot R\mathbf{v} = -2\gamma(v_y^2 +$

$v_z^2) = 0$, which is the x -axis. The breakdown condition $\nabla f|_{\mathbf{v}_b} \propto \mathbf{v}_b$ yields the entire (x, y) plane but excludes the x -axis (the set of stable points). For unstable points, we have $\dot{P}_D(\mathbf{v}) = -2\gamma(v_y^2 + v_z^2) < 0$. Thus, as a consequence of Proposition 9, any trajectory with a decreasing trajectory purity can be realized. Consequently, all trajectories with a fixed non-zero coherence f_0 and monotonically decreasing v_z component can be realized as f -preserving trajectories.

Remarkably, it is possible to reach a stable point (the x -axis) under the bit-flip channel while staying on the level set. Namely, a trajectory that lies on the cylindrical level set, has a decreasing $|v_z|$ component, and ends on the x -axis satisfies Proposition 9. Therefore, such a trajectory has a control Hamiltonian that realizes such a trajectory; see Appendix D 1 for a derivation of the corresponding control Hamiltonian. This requires enforcing $\alpha_2 \neq 0$ in Eq. (34).

On the other hand, trajectories that do not terminate on the x -axis instead end up at a breakdown point in the (x, y) plane. As we show in Appendix D 1, working with Eq. (33) while setting the other components (α_2 and α_3) of \mathbf{h} to 0, we find the corresponding breakdown time to be:

$$t_b = \frac{1}{4\gamma} \ln \left((1 + \xi) \exp \left(\frac{v_z^2(0)}{\xi f_0} \right) - \xi \right), \quad (46)$$

where $\xi = v_y^2(0)/v_x^2(0)$. Thus, t_b again decreases as the bit-flip rate γ and initial coherence value f_0 grow.

Fig. 3 illustrates the two types of trajectories described above: any trajectory that terminates at a stable point has an infinite breakdown time, and conversely, any trajectory that terminates at a breakdown point has a finite breakdown time. Fig. 4 shows the time-dependence

of the Bloch vector components along with the components of the control Hamiltonian in the latter case. The h_x and h_y components diverge at the breakdown time, where $v_z = 0$.

4. Depolarization

The depolarizing channel is defined via $\mathcal{L}_D(\rho) = \frac{1}{3} \sum_{\alpha \in \{x,y,z\}} \gamma(\sigma^\alpha \rho \sigma^\alpha - \rho)$. This corresponds to $R = -\frac{4}{3}\gamma I$ and $\mathbf{c} = \mathbf{0}$. The stable points [Eqs. (28) and (29)] are given by $\dot{P} = -\frac{4}{3}\gamma v^2 = 0$, which is the origin $\mathbf{v} = \mathbf{0}$. For unstable points, $-\frac{4}{3}\gamma v^2 < 0$. As a consequence of Proposition 9, any trajectory with a decreasing trajectory purity can be realized. If the trajectory has a fixed coherence magnitude, it can be realized as an f -preserving trajectory. The set of breakdown points is the entire (x, y) plane, excluding the origin (the stable point). Since f -preserving trajectories must have a monotonically decreasing $v_z(t)$, they must terminate at a breakdown point given that the initial state had non-zero coherence.

The breakdown time is the time it takes to reach the (x, y) plane. The calculation is identical to the one leading to Eq. (45), except that now we obtain $\dot{v}_z^2 = -\frac{8}{3}\gamma(f_0 + v_z^2)$, whose solution is $v_z(t) = [(f_0 + v_z^2(0)) e^{-\frac{8\gamma t}{3}} - f_0]^{1/2}$. Setting $v_z(t_b) = 0$ yields the breakdown time as

$$t_b = \frac{3}{8\gamma} \ln \left(\frac{v_z^2(0)}{f_0} + 1 \right), \quad (47)$$

which is again independent of the Bloch vector trajectory.

5. Relaxation

So far, we have considered examples of unital channels. We next analyze the case of relaxation, which is non-unital ($\mathbf{c} \neq \mathbf{0}$). For relaxation subject to coupling to a thermal environment at inverse temperature β (also known as generalized amplitude damping), the Lindblad operators are σ^- and σ^+ with respective rates $\gamma_- = \gamma p_0$ (relaxation) and $\gamma_+ = \gamma(1 - p_0)$ (absorption), where $p_0 = [1 + \exp(-\beta\Delta)]^{-1}$ is the ground state probability for a qubit with energy gap Δ at inverse temperature β , and γ is the relaxation rate at zero temperature. In this case, $R = \text{diag}(-\gamma/2, -\gamma/2, -\gamma)$ and $\mathbf{c} = (0, 0, 2\gamma a)$, where $a = p_0 - 1/2$. The stable points $\dot{P} = \mathbf{v} \cdot (R\mathbf{v} + \mathbf{c}) = 0$ are given by the ellipsoid $\frac{1}{2}v_x^2 + \frac{1}{2}v_y^2 + (v_z - a)^2 = a^2$, centered at $(0, 0, a)$ with major axis $\sqrt{2}a$ along v_x and v_y , and minor axis a along v_z . Since the ellipsoid touches the origin, the set of breakdown points is the entire (x, y) plane except the origin. At all points inside this ‘‘stability ellipsoid’’, the dissipator-induced purity increases [$\dot{P}_D(\mathbf{v}) > 0$] while outside, it decreases. As a consequence of Proposition 9, any trajectory for which the trajectory purity increases inside the ellipsoid and decreases outside can be realized.

As illustrated in Fig. 5, the initial state determines whether a stable point is reachable (i.e., whether the breakdown time is infinite). In particular, when the initial state has (i) coherence magnitude $f_0 = v_x^2 + v_y^2 < 2a^2$, is outside the stability ellipsoid and in the northern hemisphere (dark green) or (ii) is inside the stability ellipsoid (light green), the state can end up at a stable point on the stability ellipsoid. The purity increases for initial points inside the stability ellipsoid and decreases for initial points outside it. When the level set has a radius larger than $\sqrt{2}a$ (major axis of the stability ellipsoid), every point on the level set ends up at a breakdown point. For these initial states, the breakdown time can be found analytically and is given by Eq. (48) below.

6. Dephasing + Relaxation

If the dephasing rate is γ_d and the relaxation rate is γ_1 , the combined dissipator is $R = \text{diag}(-\gamma_2, -\gamma_2, -\gamma_1)$ and $\mathbf{c} = (0, 0, 2\gamma_1 a)$, where $\gamma_2 = 2\gamma_d + \gamma_1/2$, and $a = [1 + \exp(-\beta\Delta)]^{-1} - 1/2$ as in the pure relaxation case. The region of stable points is then the ellipsoid $\gamma_2(v_x^2 + v_y^2) + \gamma_1(v_z - a)^2 = \gamma_1 a^2$, centered at $(0, 0, a)$. The presence of dephasing, therefore, simply shrinks the stability ellipsoid for pure relaxation in the (x, y) plane.

The landscape of stable points follows the same structure as that of pure relaxation: when the initial state has (i) coherence $f_0 \equiv v_x^2 + v_y^2 < a^2 \frac{\gamma_1}{\gamma_2}$, is outside the stability ellipsoid and in the northern hemisphere or (ii) is inside the stability ellipsoid, the state will end up at a stable point on the stability ellipsoid. For states with $f_0 > a^2 \frac{\gamma_1}{\gamma_2}$, all trajectories necessarily end up at a breakdown point. We show in Appendix D 2, using Eq. (33), that in this case the breakdown time is given by

$$t_b = \frac{1}{2\gamma_1} \log \left(\frac{(v_z(0) - a)^2 + \Omega^2}{a^2 + \Omega^2} \right) + \frac{a}{\Omega\gamma_1} \left(\arctan \frac{v_z(0) - a}{\Omega} + \arctan \frac{a}{\Omega} \right), \quad (48)$$

where $\Omega^2 \equiv \frac{\gamma_2}{\gamma_1} f_0 - a^2$. Setting $\gamma_d = 0$ gives the breakdown time for the pure relaxation case of Section IV A 5, with $\gamma_2 = \gamma_r/2$ and Ω correspondingly modified.

Similarly, for points below the stability ellipsoid (i.e., $\gamma_2(v_x^2 + v_y^2) + \gamma_1(v_z - a)^2 > \gamma_1 a^2$, $f_0 < a^2(\gamma_1/\gamma_2)$ and $v_z < a$), we obtain:

$$t_b = \frac{1}{2\gamma_1} \log \left(\frac{(v_z(0) - a)^2 - \Omega^2}{a^2 - \Omega^2} \right) - \frac{a}{\Omega\gamma_1} \left(\text{arctanh} \frac{v_z(0) - a}{\Omega} + \text{arctanh} \frac{a}{\Omega} \right). \quad (49)$$

where $\Omega^2 \equiv -(\frac{\gamma_2}{\gamma_1} f_0 - a^2)$.

B. Fidelity

We now set the target quantity to be the Uhlmann fidelity $F^2(\rho, \sigma)$ between two states ρ and σ . We show in Appendix C that in terms of the corresponding Bloch vectors, the fidelity becomes $f \equiv F^2(\mathbf{v}, \mathbf{w}) = \frac{1}{2}(1 + \mathbf{v} \cdot \mathbf{w} + [(1 - \|\mathbf{v}\|^2)(1 - \|\mathbf{w}\|^2)]^{1/2})$. Thus, the fidelity, like the coherence, evades the no-go result of Proposition 1: it is a function not only of $\|\mathbf{v}\|$.

1. Level set and breakdown points

The level set for fidelity is a complex surface, but when $\|\mathbf{w}\| = 1$, it simplifies to a plane, as indicated in Figs. 1(d) to 1(f) by the yellow surface. To identify the breakdown points, we first compute ∇f :

$$\nabla f = \frac{1}{2}(\mathbf{w} - k_0 \mathbf{v}), \quad k_0 = \left[\frac{(1 - \|\mathbf{w}\|^2)}{(1 - \|\mathbf{v}\|^2)} \right]^{1/2}. \quad (50)$$

Thus, $\nabla f \times \mathbf{v} = \frac{1}{2}(\mathbf{w} \times \mathbf{v})$, and using Eq. (36):

$$\alpha_3 = \frac{(\mathbf{w} - k_0 \mathbf{v}) \cdot (R\mathbf{v} + \mathbf{c})}{\|\mathbf{w} \times \mathbf{v}\|^2}. \quad (51)$$

It follows that it is not possible to preserve the fidelity if either ($\|\mathbf{v}\| = 1$ and $\|\mathbf{w}\| \neq 1$) or $\mathbf{v} \propto \mathbf{w}$.

For $\|\mathbf{w}\| = 1$, the set of points where $\nabla f \propto \mathbf{v}$ is $\mathbf{v} = c\mathbf{w}$ for any $c \in [-1, 1]$. The breakdown points are therefore $\{c\mathbf{w} : c \in [-1, 1]\}$ minus the set of stable points. The latter set depends on the noise models, which we consider next. Henceforth, we consider the simplifying assumption $\|\mathbf{w}\| = 1$.

For further analysis, we decompose the Bloch vector \mathbf{v} as the sum of vectors parallel to and perpendicular to \mathbf{w} : $\mathbf{v} = \alpha_w \mathbf{w} + \alpha_p \mathbf{p}$ where $\mathbf{p} \cdot \mathbf{w} = 0$, $\|\mathbf{p}\| = 1$ and $\alpha_p|_{t=0} > 0$. Since the target property simplifies to $f = \frac{1}{2}(1 + \mathbf{v} \cdot \mathbf{w}) = \frac{1}{2}(1 + \alpha_w)$ for $\|\mathbf{w}\| = 1$, only α_p and the direction of \mathbf{p} can be t -dependent. To further simplify the analysis, we also assume that the fidelity-preserving Hamiltonian enforces a trajectory where the direction of \mathbf{p} is fixed (we call this a *fixed- \mathbf{p} Hamiltonian*). The constraint equation then simplifies to

$$\alpha_p \mathbf{p} = 2\mathbf{h} \times \mathbf{v} + R\mathbf{v} + \mathbf{c}. \quad (52)$$

Taking the dot product with \mathbf{v} yields

$$\alpha_p \dot{\alpha}_p = \mathbf{v} \cdot (R\mathbf{v} + \mathbf{c}) = \dot{P}_D(\mathbf{v}). \quad (53)$$

Multiplying Eq. (52) by α_p and substituting Eq. (53) gives

$$\mathbf{v} \cdot (R\mathbf{v} + \mathbf{c})\mathbf{p} = 2\alpha_p \mathbf{h} \times \mathbf{v} + \alpha_p (R\mathbf{v} + \mathbf{c}). \quad (54)$$

Comparing the coefficients of each of the orthogonal components \mathbf{w} , \mathbf{p} and $\mathbf{w} \times \mathbf{p}$ then gives the corresponding control Hamiltonian \mathbf{h} as a function of the instantaneous state.

2. Dephasing/Bit-flip

The stable point locus is the z -axis for dephasing and the x -axis for the bit flip channel, as in the discussion on coherence preservation in Section IV A. Fig. 6 illustrates that the initial conditions decide whether the state can reach a stable point. Contrasting Figs. 6(a) and 6(b) in particular, shows that it is possible to reach a stable point if an appropriate Hamiltonian is chosen, provided the initial fidelity is sufficiently low. The set of all points that can lead to stable points forms a cylinder oriented along \mathbf{w} minus cones with axis \mathbf{w} and edge along the dephasing axis. In comparison, Fig. 6(c) shows the smaller set of points that terminate at a stable point for the same initial fidelity as in Fig. 6(a) when we are constrained to apply the fixed- \mathbf{p} Hamiltonian described above.

Fig. 7 shows the time-dependence of the Bloch vector components and the control Hamiltonian components. Similarly to Fig. 4, the h_x and h_y components diverge at the breakdown time, where $v_x = v_z = 0$.

Continuing our analysis with a fixed- \mathbf{p} Hamiltonian, the dissipator can be written as

$$R\mathbf{v} + \mathbf{c} = -2\gamma[\mathbf{v} - (\mathbf{v} \cdot \hat{\mathbf{d}})]\hat{\mathbf{d}}, \quad (55)$$

where $\hat{\mathbf{d}}$ represents the unit vector in the v_z and v_x direction for the dephasing and bit-flip channels, respectively. Then Eq. (53) simplifies to

$$\alpha_p \dot{\alpha}_p = -2\gamma[\|\mathbf{v}\|^2 - (\mathbf{v} \cdot \hat{\mathbf{d}})^2] = \dot{P}_D(\mathbf{v}), \quad (56)$$

which is non-positive by the Cauchy-Schwartz inequality. As a consequence of Proposition 9, a trajectory with non-increasing purity can be realized. Since α_w remains constant to preserve fidelity, α_p should be the non-increasing component.

Recall that $\mathbf{v} = \alpha_w \mathbf{w} + \alpha_p \mathbf{p}$, $\mathbf{p} \cdot \mathbf{w} = 0$, and $\|\mathbf{w}\| = \|\mathbf{p}\| = 1$; setting $\mathbf{p} \cdot \hat{\mathbf{d}} = \cos \theta_p$ and $\mathbf{w} \cdot \hat{\mathbf{d}} = \cos \theta_w$, we have:

$$\alpha_p \dot{\alpha}_p = -2\gamma(\alpha_p^2 \sin^2 \theta_p + \alpha_w^2 \sin^2 \theta_w - 2\alpha_w \alpha_p \cos \theta_p \cos \theta_w). \quad (57)$$

This differential equation can be solved analytically for $\alpha_p(t)$ based on initial conditions. If α_w is 0, the system decays to a stable point, leading to an infinite breakdown time. Otherwise, if $\theta_p = 0$ then $\theta_w = \pi/2$ and $\alpha_p(t)^2 - \alpha_p(0)^2 = -4\gamma\alpha_w t$, which gives the breakdown time $t_b = \alpha_p(0)^2 / (4\gamma\alpha_w)$. The analysis for $\theta_p \neq 0$, including cases with finite and infinite t_b , is provided in Appendix E 2.

Note that the infinite t_b result is in contrast to the no-go coherence-preservation result we obtained for the dephasing channel: under no circumstance is it possible to indefinitely preserve the coherence of a state, except for the trivial coherence value of 0. But the fidelity can be preserved indefinitely for an appropriate choice of \mathbf{w} and initial fidelity value.

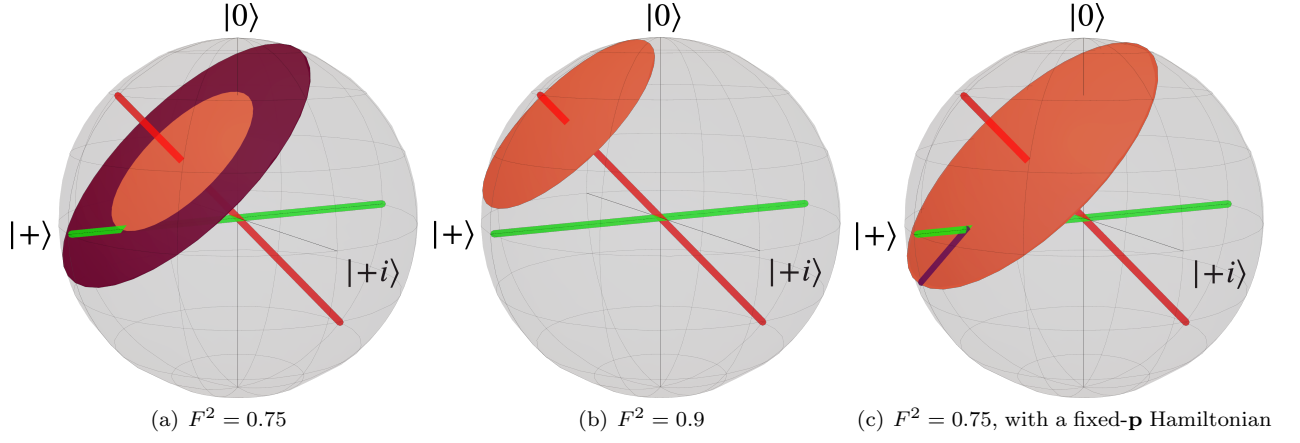


FIG. 6. Initial state stability landscape for preserving the fidelity with $\mathbf{w} = (1/\sqrt{2}, 0, 1/\sqrt{2})$, for three different initial fidelity values, subject to the bit-flip channel. The red (green) region is the set of breakdown (stable) points. The level sets of constant fidelity are the orange and purple (a,c) and orange (b) regions inside the Bloch sphere, which form a plane. The purple regions represent initial states that can lead to stable points, while the orange regions represent initial states guaranteed to lead to breakdown.

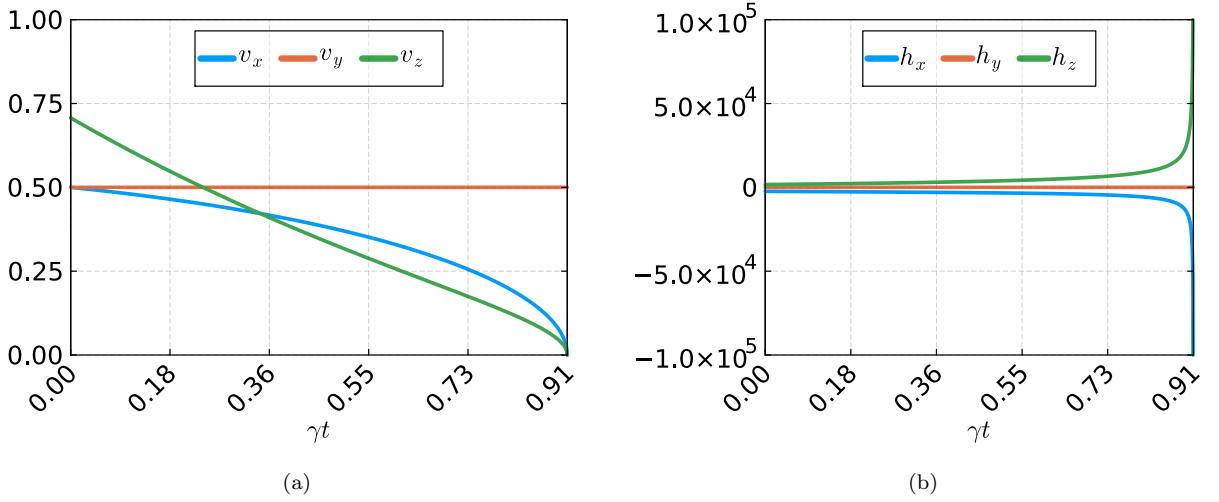


FIG. 7. Time dependence of the Bloch vector components (a) and the control Hamiltonian components (b) for preserving the fidelity at a value of $F^2 = 0.75$ with respect to $\mathbf{w} = (0, 1, 0)$ subject to the bit-flip channel, using only the necessary component of the f -preserving Hamiltonian [Eq. (33)]. The initial state is $(1/2, 1/2, 1/\sqrt{2})$. Note that the Hamiltonian diverges near the breakdown point ($v_x = v_z = 0$).

3. Depolarization

The set of stable points contains only one point: the origin. The state can reach the origin given that we start with $\alpha_w = 0$, which leads to an infinite breakdown time. Otherwise, repeating the same analysis as in the previous section, setting $R\mathbf{v} + \mathbf{c} = -4\gamma\mathbf{v}/3$ yields

$$\alpha_p \dot{\alpha}_p = -\frac{4\gamma}{3}(\alpha_p^2 + \alpha_w^2). \quad (58a)$$

This gives

$$\alpha_p^2(t) = e^{-8\gamma t/3}(\alpha_p^2(0) + \alpha_w^2) - \alpha_w^2. \quad (59)$$

Setting $\alpha_p(t_b) = 0$ gives the breakdown time

$$t_b = \frac{3}{8\gamma} \ln \frac{\alpha_p^2(0) + \alpha_w^2}{\alpha_w^2} = \frac{3}{8\gamma} \ln \frac{\|\mathbf{v}(0)\|^2}{(\mathbf{v} \cdot \mathbf{w})^2}. \quad (60)$$

The behavior matches that of coherence preservation: t_b is independent of the control Hamiltonian used. However, not all initial states will lead to a finite t_b .

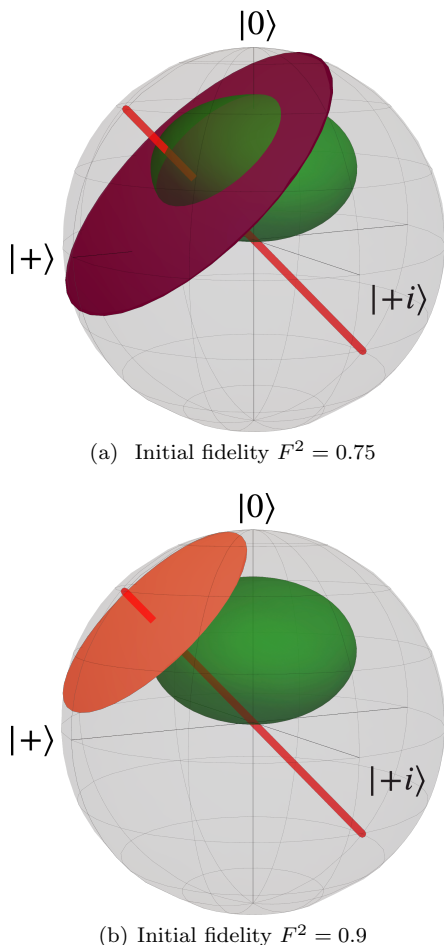


FIG. 8. Initial state stability landscape for preserving the fidelity with $\mathbf{w} = (1/\sqrt{2}, 0, 1/\sqrt{2})$, for two different initial fidelity values, subject to the relaxation channel with $\beta\Delta = 2$. The red (green) region is the set of breakdown (stable) points. The level sets of constant fidelity are the purple (a) and orange (b) regions inside the Bloch sphere, which form a plane. The purple regions represent initial states that can lead to stable points, while the orange regions represent initial states guaranteed to lead to breakdown.

4. Relaxation

The set of stable points forms an ellipsoid. Following the same notation as in Section IV A 5, the dissipative part can be written as $R\mathbf{v} + \mathbf{c} = -\frac{\gamma}{2}\mathbf{v} + \frac{\gamma}{2}(4a - \mathbf{v} \cdot \hat{\mathbf{k}})\mathbf{k}$, where $\hat{\mathbf{k}}$ is the unit vector in v_z direction. Then Eq. (53) simplifies to

$$\alpha_p \dot{\alpha}_p = -\frac{\gamma}{2}(\|\mathbf{v}\|^2 - 4a(\mathbf{v} \cdot \hat{\mathbf{k}}) + (\mathbf{v} \cdot \hat{\mathbf{k}})^2). \quad (61)$$

Since $\|\mathbf{v}\|^2 = \alpha_p^2 + \alpha_w^2$ and $\mathbf{v} \cdot \hat{\mathbf{k}} = \alpha_p(\mathbf{p} \cdot \hat{\mathbf{k}}) + \alpha_w(\mathbf{w} \cdot \hat{\mathbf{k}})$ where $\mathbf{p} \cdot \hat{\mathbf{k}}$ and $\mathbf{w} \cdot \hat{\mathbf{k}}$ are constant, the resulting differential equation is also solvable analytically for a given initial condition. Next, we discuss how varying initial conditions lead to different dynamics.

Fig. 8 illustrates how the initial state determines whether a stable point can be reached. If the fidelity level set intersects the region of stable points, as in Fig. 8(a), then stable points are reachable from any initial state on that level set (except when the initial state is collinear with \mathbf{w}). This unique control landscape allows us to preserve the fidelity for almost all states on a level set, unlike any of our previous examples. Surprisingly, they are reachable using the simple fixed- \mathbf{p} Hamiltonian. Contrast this with the case of the dephasing channel, where using the fixed- \mathbf{p} Hamiltonian limited the set of reachable stable points. For points starting inside the ellipsoid, the purity increases (i.e., α_p increases) until the ellipsoid is reached. Similarly, for points starting outside the ellipsoid, the purity decreases (i.e., α_p decreases), and eventually, the state ends up on the ellipsoid.

In contrast, when the level set does not intersect the stability ellipsoid, all initial states necessarily reach a breakdown point, as illustrated in Fig. 8(b).

V. CONCLUSIONS AND OUTLOOK

We have presented a tracking control framework for using smoothly time-varying Hamiltonians to address quantum property preservation (QPP): the preservation of key target properties (e.g., coherence and fidelity) of open quantum systems. QPP can be interpreted as providing operational stability to a quantum system, a softer requirement than preserving the entire state over time. The main advantages of our tracking control approach over standard quantum error avoidance, correction, or suppression are that it avoids any encoding overhead, does not require any measurement-based feedback, and is applicable even subject to Markovian environments, where traditional Hamiltonian control approaches such as dynamical decoupling fail.

We found necessary conditions for control Hamiltonians to preserve a given target property f over time, and provided analytic (non-unique) solutions for these Hamiltonians. We showed that independent of the initial state, the dissipator delineates certain regions in the state space where stability is guaranteed to persist indefinitely (stable points). Similarly, given a dissipator, the target property f generates instability regions in the state space (breakdown points). Breakdown points are associated with a breakdown time at which the Hamiltonian diverges and after which the preservation of f ceases. The goal of property preservation can, therefore, be viewed as preventing the state trajectory from passing through any breakdown point. However, the set of possible f -preserving trajectories is also constrained; it is characterized by whether the control Hamiltonian can counteract the dissipator action and result in unitary dynamics.

As we have defined it here, one obvious limitation of the tracking control approach to QPP is that it requires full knowledge of the state ρ . For an unknown state, this

would, in principle, necessitate full quantum state tomography, a computationally demanding requirement even when implemented using methods such as compressed sensing [53]. An important potential avenue for simplification is the use of shadow tomography, which requires exponentially fewer measurements than full state tomography and provides partial information about the quantum state [54, 55]. Future work will address whether the tracking control problem can be reformulated using such partial state information.

An additional potential future simplification is related to the fact that we have presented a time-local formulation of the target preservation control problem. A natural reformulation in terms of minimizing the integrated deviation of the target property from its initial value is an interesting question. It may even sidestep the issue of the breakdown singularities of the tracking control method.

Other avenues for future research include establishing connections to quantum error avoidance and correction by allowing for the use of ancilla qubits. While this direction is orthogonal to the spirit of the quantum property preservation framework outlined in the Introduction, it is nevertheless potentially promising as an avenue for reducing the resource requirements typically assumed in quantum error correction. For example, consider developing a tracking control framework that uses partial state information to implement a codespace-preserving Hamiltonian for stabilizer codes. In this context, we may choose the target function to be the fidelity of the input state with the +1 eigenspace of the stabilizer group and seek a control Hamiltonian that ensures the fidelity remains high until the next error correction cycle.

ACKNOWLEDGMENTS

This research was supported by the ARO MURI grant W911NF-22-S-0007. KS acknowledges support from the Graduate Student Fellowship awarded by USC Viterbi School of Engineering. We thank Parth Darekar for many helpful discussions during the early stages of this work.

Appendix A: Coherence vector

We closely follow the exposition in [47], which also contains the proofs of all the propositions provided below.

Let $M(d, F)$ denote the vector space of $d \times d$ matrices with coefficients in F , where $F \in \{\mathbb{R}, \mathbb{C}\}$. For our purposes it suffices to identify $\mathcal{B}(\mathcal{H})$ with $M(d, \mathbb{C})$. Elements of $\mathcal{B}[\mathcal{B}(\mathcal{H})]$, i.e., linear transformations $\mathcal{E} : \mathcal{B}(\mathcal{H}) \rightarrow \mathcal{B}(\mathcal{H})$, are called superoperators, or maps.

Given a nice operator basis $\{F_j\}$, we may “coordinate” the operator $X \in \mathcal{B}(\mathcal{H})$ as

$$X = \sum_{j=0}^J \mathbf{X}_j F_j, \quad (\text{A1})$$

where $J \equiv d^2 - 1$ and we use the notation $\mathbf{X} = \{\mathbf{X}_j\}$ for the vector of coordinates of the operator X (we interchangeably use the \vec{X} and \mathbf{X} notations to denote a vector). I.e., for any $X \in \mathcal{B}(\mathcal{H})$:

$$\mathbf{X}_i = \langle F_i, X \rangle = \text{Tr}(F_i X). \quad (\text{A2})$$

The matrix elements of a *superoperator* $\mathcal{E} : \mathcal{B}(\mathcal{H}) \rightarrow \mathcal{B}(\mathcal{H})$ are given by

$$\mathcal{E}_{ij} = \langle F_i, \mathcal{E}(F_j) \rangle = \text{Tr}[F_i \mathcal{E}(F_j)]. \quad (\text{A3})$$

Definition 13. \mathcal{E} is Hermiticity-preserving iff:

$$[\mathcal{E}(A^\dagger)]^\dagger = \mathcal{E}(A) \quad \forall A \in \mathcal{B}(\mathcal{H}). \quad (\text{A4})$$

\mathcal{E} is Hermitian iff

$$\mathcal{E}^\dagger(A) = \mathcal{E}(A) \quad \forall A \in \mathcal{B}(\mathcal{H}). \quad (\text{A5})$$

Proposition 10. The operator $X \in \mathcal{B}(\mathcal{H})$ is Hermitian iff $\mathbf{X} \in \mathbb{R}^{d^2}$ in a nice operator basis. \mathcal{E} is Hermiticity-preserving iff $\mathcal{E} \in M(d^2, \mathbb{R})$. The Liouvilian is Hermiticity-preserving.

Corollary 3. The quantum master equation $\dot{\rho} = \mathcal{L}\rho$ in a nice operator basis is a real-valued linear ordinary differential equation for the vector $\boldsymbol{\rho}$ whose coordinates are $\rho_j = \text{Tr}(\rho F_j)$:

$$\dot{\boldsymbol{\rho}} = \mathcal{L}\boldsymbol{\rho}, \quad \boldsymbol{\rho} \in \mathbb{R}^{d^2}, \quad \mathcal{L} \in M(d^2, \mathbb{R}). \quad (\text{A6})$$

Proof. This follows directly from Proposition 10 with $X = \rho$ and $\mathcal{E} = \mathcal{L}$. \square

By Corollary 3, we can expand the density matrix in the nice operator basis as:

$$\rho = \mathbf{F}' \cdot \boldsymbol{\rho} = \frac{1}{d}I + \mathbf{F} \cdot \mathbf{v}, \quad (\text{A7})$$

where $\mathbf{F}' = (F_0, F_1, \dots, F_J)$, $\boldsymbol{\rho} = (1/\sqrt{d}, v_1, \dots, v_J)^T$, $\mathbf{F} = (F_1, \dots, F_J)$ collects the traceless basis-operators into a vector, and the corresponding coordinate vector $\mathbf{v} = (v_1, \dots, v_J)^T \in \mathbb{R}^J$ is called the *coherence vector*. We have:

$$v_j = \text{Tr}(\rho F_j) = \rho_j. \quad (\text{A8})$$

The space of coherence vectors for a d -dimensional quantum system (qudit) is a convex set $\mathcal{M}^{(d)}$ that is topologically equivalent to a sphere. For $d = 2$ (a qubit), $\mathcal{M}^{(2)}$ is a sphere. For $d > 2$, $\mathcal{M}^{(d)}$ is still a convex set but is no longer a sphere, nor is it a polytope. Instead, its faces are copies of $\mathcal{M}^{(d')}$ with $d' < d$. The boundary of $\mathcal{M}^{(d)}$ contains all states of less than maximal rank. The set $\mathcal{M}^{(d)}$ lies inside a sphere of radius $\sqrt{(d-1)/(2d)}$ and contains a maximal sphere of radius $\sqrt{1/[2d(d-1)]}$ [46].

Proposition 11. *The coherence vector satisfies Eq. (2). Moreover, the decomposition of \mathcal{L} as $\mathcal{L} = \mathcal{L}_H + \mathcal{L}_D$ with \mathcal{L}_H and \mathcal{L}_D given by Eqs. (1b) and (1c) induces the decomposition $\mathcal{L}_H(\rho) \rightsquigarrow Q\mathbf{v}$, $\mathcal{L}_D(\rho) \rightsquigarrow R\mathbf{v} + \mathbf{c}$, $\mathbf{c} \in \mathbb{R}^J$, $R, Q \in M(J, \mathbb{R})$, and $Q = -Q^T$ (anti-symmetric). Specifically, R , Q , and \mathbf{c} have elements in the nice operator basis $\{F_j\}$ given by:*

$$Q_{ij} \equiv \text{Tr}[F_i \mathcal{L}_H(F_j)] = Q_{ij}^* \quad (\text{A9a})$$

$$R_{ij} \equiv \text{Tr}[F_i \mathcal{L}_D(F_j)] = R_{ij}^* \quad (\text{A9b})$$

$$c_j = \frac{1}{d} \text{Tr}[F_j \mathcal{L}_D(I)] = c_j^* . \quad (\text{A9c})$$

Definition 14. *The dissipator \mathcal{L}_D is unital if $\mathcal{L}_D(I) = 0$.*

Proposition 12. *$\mathbf{c} = \mathbf{0}$ iff \mathcal{L}_D is unital.*

Proposition 13. *The following are conditions under which R is symmetric:*

1. *R is symmetric in the single qubit ($d = 2$) case.*
2. *R is symmetric and $\mathbf{c} = \mathbf{0}$ iff the Lindblad operators \mathcal{L}_α are Hermitian.*

Appendix B: The Bloch vector

We write $\sigma^0 = I$. The set of Pauli matrices $\{\sigma^0, \sigma^x, \sigma^y, \sigma^z\}$ forms a basis for the space of 2×2 complex matrices. It is not a proper nice operator basis since it is not normalized, and this gives rise to the difference between the Bloch vector and the coherence vector for a qubit. In more detail, any qubit density matrix can be expanded in the Pauli basis as

$$\rho = \frac{1}{2} \left(I + \sum_{i=x,y,z} v_i \sigma^i \right) = \frac{1}{2} (I + \mathbf{v} \cdot \boldsymbol{\sigma}) , \quad (\text{B1})$$

where $\mathbf{v} = (v_x, v_y, v_z) \in S^2$ is called the *Bloch vector*, S^2 is the unit sphere in \mathbb{R}^3 , and $\boldsymbol{\sigma} = (\sigma^x, \sigma^y, \sigma^z)$ is the vector of Pauli matrices. Since the Pauli matrices are traceless and $\text{Tr} I = 2$, the expansion ensures that $\text{Tr} \rho = 1$. Since the Pauli matrices are Hermitian, this also ensures that ρ is Hermitian. In terms of the Bloch vector, ρ becomes

$$\rho = \frac{1}{2} \begin{pmatrix} 1 + v_z & v_x - i v_y \\ v_x + i v_y & 1 - v_z \end{pmatrix} . \quad (\text{B2})$$

Positivity is the statement that the eigenvalues λ_\pm are non-negative:

$$|\rho - \lambda I| = 0 \Rightarrow \lambda^2 - (\text{Tr} \rho) \lambda + |\rho| = 0 , \quad (\text{B3})$$

where $|\rho|$ denotes the determinant of ρ . I.e., using $\text{Tr} \rho = 1$:

$$\lambda_\pm = \frac{1}{2} (1 \pm \sqrt{1 - 4|\rho|}) \geq 0 . \quad (\text{B4})$$

Positivity can now be made explicit by noting that

$$|\rho| = \frac{1}{4} (1 - v_z^2 - (v_x^2 + v_y^2)) = \frac{1}{4} (1 - \|\mathbf{v}\|^2) , \quad (\text{B5})$$

so that by Eq. (B4): $\lambda_\pm = \frac{1}{2} (1 \pm \|\mathbf{v}\|)$. Thus, positivity is equivalent to:

$$\|\mathbf{v}\| \leq 1 , \quad (\text{B6})$$

which means that valid qubit states are represented by Bloch vectors that lie on the surface or in the interior of the unit sphere.

For a qubit, expanding the Hamiltonian in the Pauli basis as $H = h_0 I + \mathbf{h} \cdot \boldsymbol{\sigma}$ yields:

$$\mathcal{L}_H(\rho) = -i[H, \rho] = -\frac{i}{2} \sum_{i \in \{x,y,z\}} h_i [\sigma^i, \mathbf{v} \cdot \boldsymbol{\sigma}] \quad (\text{B7a})$$

$$= -\frac{i}{2} \sum_{i,j \in \{x,y,z\}} h_i v_j [\sigma^i, \sigma^j] \quad (\text{B7b})$$

$$= \sum_{i,j,k \in \{x,y,z\}} \varepsilon_{ijk} h_i v_j \sigma^k = (\mathbf{h} \times \mathbf{v}) \cdot \boldsymbol{\sigma} . \quad (\text{B7c})$$

Since $\dot{\rho} = \frac{1}{2} (\dot{\mathbf{v}} \cdot \boldsymbol{\sigma})$, we find $\dot{\mathbf{v}} \cdot \boldsymbol{\sigma} = 2(\mathbf{h} \times \mathbf{v}) \cdot \boldsymbol{\sigma}$, so that:

$$Q\mathbf{v} = \dot{\mathbf{v}} = 2(\mathbf{h} \times \mathbf{v}) . \quad (\text{B8})$$

Table II provides the dissipators for various common noise channels we study in this work. These are calculated using Eq. (A9), after adjusting for the difference in normalization.

Noise channel	Dissipator $D = (R, \mathbf{c})$
Dephasing (Z)	$R = \text{diag}(-2\gamma, -2\gamma, 0)$, $\mathbf{c} = \mathbf{0}$
Bit-flip (X)	$R = \text{diag}(0, -2\gamma, -2\gamma)$, $\mathbf{c} = \mathbf{0}$
Bit-phase-flip (Y)	$R = \text{diag}(-2\gamma, 0, -2\gamma)$, $\mathbf{c} = \mathbf{0}$
Depolarizing	$R = -\frac{4}{3}\gamma I$, $\mathbf{c} = \mathbf{0}$
Relaxation at temperature T	$R = (-\frac{\gamma}{2}, -\frac{\gamma}{2}, -\gamma)$, $\mathbf{c} = (0, 0, 2\gamma a)$
Relaxation at temperature T (γ_1) + Dephasing (γ_d)	$R = (-\gamma_2, -\gamma_2, -\gamma_1)$, $\mathbf{c} = (0, 0, 2\gamma_1 a)$

TABLE II. Dissipators for different noise channels. $\gamma_2 \equiv 2\gamma_d + \frac{\gamma_1}{2}$, $a \equiv [1 + \exp(-\beta\Delta)]^{-1} - 1/2$ where Δ is the qubit energy gap and $\beta = 1/T$ is the inverse temperature.

Appendix C: Uhlmann fidelity between Bloch vectors

The Uhlmann fidelity between two general density matrices is $F(\rho, \chi) = \|\sqrt{\rho}\sqrt{\chi}\|_1 = \text{Tr}(\sqrt{\sqrt{\chi}\rho\sqrt{\chi}})$.

Proposition 14. *In the case of two qubits, the Uhlmann fidelity expressed in terms of the respective Bloch vectors \mathbf{v} and \mathbf{w} of ρ and χ is:*

$$F^2(\mathbf{v}, \mathbf{w}) = \frac{1}{2} \left(1 + \mathbf{v} \cdot \mathbf{w} + [(1 - \|\mathbf{v}\|^2)(1 - \|\mathbf{w}\|^2)]^{1/2} \right). \quad (\text{C1})$$

Proof. Following Ref. [56], let A be any 2×2 positive semidefinite matrix, with eigenvalues $\lambda_1, \lambda_2 \geq 0$. Then \sqrt{A} has eigenvalues $\sqrt{\lambda_1}, \sqrt{\lambda_2} \geq 0$, so that $\text{Tr}\sqrt{A} = \sqrt{\lambda_1} + \sqrt{\lambda_2}$ and $\det(A) = \lambda_1 \lambda_2$. Thus:

$$(\text{Tr}\sqrt{A})^2 = \lambda_1 + \lambda_2 + 2\sqrt{\lambda_1 \lambda_2} = \text{Tr}A + 2\sqrt{\det(A)}. \quad (\text{C2})$$

Now let $A = \sqrt{\rho}\chi\sqrt{\rho}$, which is a positive semidefinite matrix since it is the product of positive semidefinite matrices. Then, using the cyclic property of the trace and the product formula for determinants, we have:

$$F^2(\rho, \sigma) = (\text{Tr}\sqrt{A})^2 = \text{Tr}(\sqrt{\rho}\chi\sqrt{\rho}) + 2\sqrt{\det(\sqrt{\rho}\chi\sqrt{\rho})} \quad (\text{C3a})$$

$$= \text{Tr}(\rho\chi) + 2\sqrt{\det(\rho\chi)}. \quad (\text{C3b})$$

Next, write $\rho = \frac{1}{2}(I + \mathbf{v} \cdot \sigma)$ and $\chi = \frac{1}{2}(I + \mathbf{w} \cdot \sigma)$. Thus,

$$\text{Tr}(\rho\chi) = \frac{1}{2}(1 + \mathbf{v} \cdot \mathbf{w}) \quad (\text{C4})$$

Using $\lambda_{\pm} = \frac{1}{2}(1 \pm \|\mathbf{v}\|)$ for the eigenvalues of ρ and the fact that the determinant is the product of the eigenvalues,

$$\det(\rho\chi) = \det(\rho)\det(\chi) = \frac{1}{16}(1 - \|\mathbf{v}\|^2)(1 - \|\mathbf{w}\|^2). \quad (\text{C5})$$

Thus, $\sqrt{\det(\rho\chi)} = \frac{1}{4}[(1 - \|\mathbf{v}\|^2)(1 - \|\mathbf{w}\|^2)]^{1/2}$, and Eq. (C1) follows from Eq. (C3). \square

Appendix D: Derivation of control Hamiltonians for coherence preservation

1. Preserving the coherence magnitude for the bit-flip channel

For later reference, we note that for $f = v_x^2 + v_y^2$:

$$\nabla f = (2v_x, 2v_y, 0) \quad (\text{D1a})$$

$$\nabla f \times \mathbf{v} = (2v_y v_z, -2v_x v_z, 0) \quad (\text{D1b})$$

$$\|\nabla f \times \mathbf{v}\|^2 = 4v_z^2 f_0^2, \quad (\text{D1c})$$

where $f_0 = v_x^2(0) + v_y^2(0)$ is the coherence magnitude that is being preserved.

We can solve the dynamics equation, for which we first need to compute $\mathbf{h} \times \mathbf{v}$ using $\mathbf{h} = \alpha_1 \mathbf{v} + \alpha_2 \nabla f + \alpha_3 \nabla f \times \mathbf{v}$ [Eq. (34)]. In doing so, the term $\alpha_1 \mathbf{v}$ drops

out, and we use $\alpha_3 = \frac{1}{2} \frac{\nabla f \cdot (R\mathbf{v} + \mathbf{c})}{\|\nabla f \times \mathbf{v}\|^2}$ [Eq. (36)] with $R = \text{diag}(0, -2\gamma, -2\gamma)$, and $\mathbf{c} = \mathbf{0}$. We then have

$$R\mathbf{v} + \mathbf{c} = (0, -2\gamma v_y, -2\gamma v_z) \quad (\text{D2a})$$

$$\nabla f \cdot (R\mathbf{v} + \mathbf{c}) = -4\gamma v_y^2. \quad (\text{D2b})$$

Thus, using Eq. (D1), we find

$$\alpha_3 = -\frac{1}{2} \frac{\gamma v_y^2}{f_0 v_z^2}, \quad (\text{D3})$$

and hence:

$$\mathbf{h} = \left(-\frac{\gamma v_y^3}{f_0 v_z} + 2\alpha_2 v_x, \frac{\gamma v_x v_y^2}{f_0 v_z} + 2\alpha_2 v_y, 0 \right), \quad (\text{D4})$$

which yields:

$$\mathbf{h} \times \mathbf{v} = \left(\frac{\gamma v_x v_y^2}{f_0} + 2\alpha_2 v_y v_z, \frac{\gamma v_y^3}{f_0} - 2\alpha_2 v_x v_z, -\frac{\gamma v_y^2}{v_z} + 2\alpha_2 v_x v_y \right). \quad (\text{D5})$$

Then, using Eq. (26a), corresponding equations for the Bloch vector components are:

$$\dot{v}_x = \frac{2\gamma v_x v_y^2}{f_0} + 4\alpha_2 v_y v_z \quad (\text{D6a})$$

$$\dot{v}_y = 2\gamma v_y \left(\frac{v_y^2}{f_0} - 1 \right) - 4\alpha_2 v_x v_z \quad (\text{D6b})$$

$$\dot{v}_z = -2\gamma \frac{v_z^2 + v_y^2}{v_z} + 4\alpha_2 v_x v_y. \quad (\text{D6c})$$

a. $\alpha_2 = 0$: finite breakdown time

For $\alpha_2 = 0$, solving Eq. (D6b) first gives:

$$v_y^2(t) = \frac{v_y^2(0) f_0}{v_x^2(0) e^{4\gamma t} + v_y^2(0)}. \quad (\text{D7})$$

This lets us solve Eq. (D6c), yielding:

$$v_z^2(t) = \frac{e^{-4\gamma t}}{v_x^2(0)} \left[v_x^2(0) v_z^2(0) - f_0 v_y^2(0) \ln \left(\frac{v_y^2(0) + e^{4\gamma t} v_x^2(0)}{f_0} \right) \right]. \quad (\text{D8})$$

In this trajectory, clearly $v_y(t) > 0 \forall t \geq 0$. Therefore the Hamiltonian [Eq. (D4)] diverges when $v_z(t) = 0$; the solution then yields Eq. (46).

b. $\alpha_2 \neq 0$: infinite breakdown time

Different values of α_2 yield different trajectories. Instead of analyzing the result of varying α_2 , we can choose a trajectory we would like the Bloch vector to take and calculate the required Hamiltonian based on that path. Such a choice can be advantageous; e.g., as we demonstrate here, we can ensure that the trajectory ends at a stable point, which means that the coherence magnitude is indefinitely preserved.

Due to Proposition 9, any trajectory can be realized as long as that trajectory's purity is the same as $\partial_u P_D$ up to a positive multiplicative factor. Consider $\partial_u P_D$ for the bit flip channel:

$$\partial_u P_D[\mathbf{l}(u)] = \mathbf{l} \cdot (R\mathbf{l} + \mathbf{c}) = -2\gamma(l_y^2 + l_z^2), \quad (\text{D9})$$

so the trajectory purity must be negative along the entire path. Since the preserved property is the coherence magnitude, the trajectory should lie on a cylindrical level set. As long as these two properties are satisfied, we can find a Hamiltonian that moves the Bloch vector along that trajectory.

For example, suppose we wish to realize a trajectory that ends with the state on the x -axis of the Bloch sphere (e.g., the curved green arrow in Fig. 3). Since the trajectory must lie on the level set, which is a cylinder with radius $\sqrt{f_0}$ (recall Section IV A 1), one possible (non-unique) trajectory that satisfies the required conditions is

$$\begin{aligned} \mathbf{l}(u) &= (l_x(u), l_y(u), l_z(u)) & (\text{D10a}) \\ &= (\sqrt{f_0} \sin\left(\frac{\pi}{2}\theta + \frac{\pi}{2}(1-\theta)u\right), \\ &\quad \sqrt{f_0} \cos\left(\frac{\pi}{2}\theta + \frac{\pi}{2}(1-\theta)u\right), v_z(0)\sqrt{1-u}), \end{aligned} \quad (\text{D10b})$$

where $u \in [0, 1]$ and $\theta = \frac{2}{\pi} \arctan(v_x(0)/v_y(0))$. If the reparameterization to physical time is given by $\varphi : [0, 1] \mapsto [0, t_f]$, the realizable trajectory is given by $\mathbf{v}(\varphi(u)) = \mathbf{l}(u)$.

Proposition 9 yields $c(u)$ (where $\varphi(s) = \int_0^s c(u)du$): the trajectory purity is $P_1(u) = \frac{1}{2}[1 + \|\mathbf{l}(u)\|^2] = \frac{1}{2}[1 + f_0 + v_z^2(0)(1-u)]$, which leads to

$$c(u) = \frac{\partial_u P_1}{\partial_u P_D} = \frac{v_z^2(0)}{4\gamma(l_y^2(u) + l_z^2(u))} = \frac{v_z^2(0)}{4\gamma(v_y^2(t) + v_z^2(t))}. \quad (\text{D11})$$

To find an appropriate value of α_2 , we can use the following relation between \mathbf{l} and \mathbf{v} :

$$\partial_u \varphi(u) \cdot \dot{\mathbf{v}}(t) = \partial_u \mathbf{l}(u) \quad (\text{D12a})$$

$$\text{or } c(u) \cdot \dot{\mathbf{v}}(t) = \partial_u \mathbf{l}(u). \quad (\text{D12b})$$

The r.h.s. of Eq. (D12b) can be computed from the trajectory information:

$$\partial_u l_x(u) = \frac{\pi}{2}(1-\theta)l_y(u) = \frac{\pi}{2}(1-\theta)v_y(t). \quad (\text{D13})$$

Equating the components of the vectors on both sides of Eq. (D12b) then yields α_2 , e.g., via Eq. (D6a):

$$\begin{aligned} &\frac{v_z^2(0)}{4\gamma(v_y^2(t) + v_z^2(t))} \left(\frac{2\gamma v_x(t)v_y^2(t)}{f_0} + 4\alpha_2 v_y(t)v_z(t) \right) \\ &= \frac{\pi}{2}(1-\theta)v_y(t), \end{aligned} \quad (\text{D14})$$

so that

$$\alpha_2 = \frac{\gamma}{2v_z(t)} \left(\frac{\pi(1-\theta)(v_y^2(t) + v_z^2(t))}{v_z^2(0)} - \frac{v_x(t)v_y(t)}{f_0} \right). \quad (\text{D15})$$

Using this result for α_2 along with Eq. (D3) for α_3 will move the Bloch vector along the prescribed trajectory while preserving the coherence. Moreover, the trajectory leads to a stable point since the endpoint is on the x -axis. The corresponding breakdown time is infinity.

2. Breakdown time for dephasing+relaxation channel in coherence preservation

Recall from Section IV A 6 that the dissipator is $R = \text{diag}(-\gamma_2, -\gamma_2, -\gamma_1)$ and $\mathbf{c} = (0, 0, 2\gamma_1 a)$, where $1/T_2 = 2\gamma_d + \gamma_1/2$ and $a = [1 + \exp(-\beta\Delta)]^{-1} - 1/2$. Thus:

$$R\mathbf{v} + \mathbf{c} = (-\gamma_2 v_x, -\gamma_2 v_y, -\gamma_1(v_z - 2a)) \quad (\text{D16a})$$

$$\nabla f \cdot (R\mathbf{v} + \mathbf{c}) = -2\gamma_2 f_0. \quad (\text{D16b})$$

Then, using Eqs. (33) and (D1) the basic control Hamiltonian ($\alpha_2 = 0$) is:

$$\mathbf{h} = -\frac{\gamma_2}{2v_z}(v_y, -v_x, 0), \quad (\text{D17})$$

and using Eq. (26a), the corresponding equations for the Bloch vector components are:

$$\dot{v}_x = 0 \quad (\text{D18a})$$

$$\dot{v}_y = 0 \quad (\text{D18b})$$

$$\dot{v}_z = -\frac{\gamma_2 f_0}{v_z} - \gamma_1 v_z + 2\gamma_1 a \quad (\text{D18c})$$

$$= -\frac{\gamma_1}{v_z} \left((v_z - a)^2 + \left(\frac{\gamma_2}{\gamma_1} f_0 - a^2 \right) \right). \quad (\text{D18d})$$

As argued in Section IV A 6, for points with $f_0 > a^2 \frac{\gamma_1}{\gamma_2}$, all trajectories necessarily end up at a breakdown point. The constant term in Eq. (D18d) is positive for such points. Substituting $\Omega^2 \equiv \frac{\gamma_2}{\gamma_1} f_0 - a^2$ and integrating, we obtain:

$$-\gamma_1 \int_0^t ds = \int_{v_z(0)}^{v_z(t)} \frac{v_z dv_z}{(v_z - a)^2 + \Omega^2} \quad (\text{D19a})$$

$$\begin{aligned} &= \frac{1}{2} \log\left((v_z - a)^2 + \Omega^2\right) \\ &\quad + \frac{a}{\Omega} \arctan \frac{v_z - a}{\Omega} \Big|_{v_z(0)}^{v_z(t)}. \end{aligned} \quad (\text{D19b})$$

Substituting $v_z(t_b) = 0$ finally gives the breakdown time as in Eq. (48), and similarly, when $f_0 < a^2(\gamma_1/\gamma_2)$ and $v_z < a$ we obtain Eq. (49).

Appendix E: Derivation of control Hamiltonians for Uhlmann fidelity preservation

1. α_3 for various noise channels

Substituting the dissipator $D = (R, \mathbf{c})$ for various noise channels into Eq. (51) yields Table III.

Noise channel	α_3
Dephasing	$-2\gamma \frac{(\mathbf{w}-k_0\mathbf{v}) \cdot (v_x, v_y, 0)}{\ \mathbf{w} \times \mathbf{v}\ ^2}$
Bit-flip	$-2\gamma \frac{(\mathbf{w}-k_0\mathbf{v}) \cdot (0, v_y, v_z)}{\ \mathbf{w} \times \mathbf{v}\ ^2}$
Depolarizing	$-\frac{4\gamma}{3} \frac{(\mathbf{w}-k_0\mathbf{v}) \cdot \mathbf{v}}{\ \mathbf{w} \times \mathbf{v}\ ^2}$
Relaxation	$-\frac{\gamma}{2} \frac{(\mathbf{w}-k_0\mathbf{v}) \cdot (v_x, v_y, 2(1-v_z))}{\ \mathbf{w} \times \mathbf{v}\ ^2}$

TABLE III. α_3 for different noise channels.

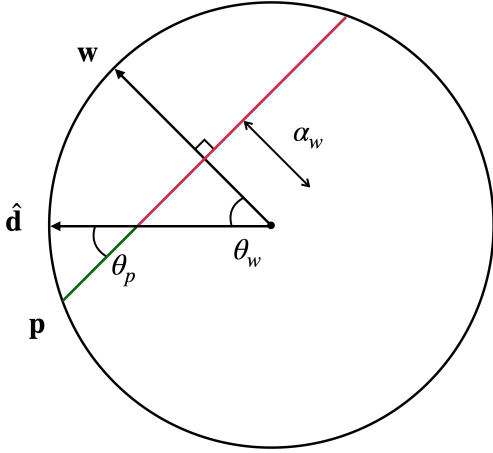


FIG. 9. Cross-sectional view of the initial states leading to stable points in Fig. 6(c).

2. Preserving Uhlmann fidelity under dephasing/bit-flip

Fig. 9 provides a simple way to characterize initial states that lead to stable points when using the fixed- \mathbf{p} Hamiltonian:

1. \mathbf{p} , \mathbf{w} and $\hat{\mathbf{d}}$ should be coplanar, i.e. $\mathbf{p} \cdot (\mathbf{w} \times \hat{\mathbf{d}}) = 0$.
2. the initial state should be on the correct side of the sphere: $\hat{\mathbf{d}}$ should lie between \mathbf{p} and \mathbf{w} , i.e., $\theta_p + \theta_w = \pi/2$ since \mathbf{p} and \mathbf{w} are orthogonal.
3. the initial state lies on the green segment in Fig. 9: $\alpha_p > \alpha_w \tan \theta_w$.

All other points have a finite breakdown point, and the corresponding breakdown time t_b can be calculated: rearranging Eq. (57) gives

$$-2\gamma = \frac{\alpha_p \dot{\alpha}_p}{\alpha_p^2 \sin^2 \theta_p + \alpha_w^2 \sin^2 \theta_w - 2\alpha_w \alpha_p \cos \theta_p \cos \theta_w} \quad (\text{E1a})$$

$$= \frac{\alpha_p \dot{\alpha}_p}{\alpha_p^2 - \alpha_p \left(\frac{2\alpha_w \cos \theta_p \cos \theta_w}{\sin^2 \theta_p} \right) + \left(\frac{\alpha_w^2 \sin^2 \theta_w}{\sin^2 \theta_p} \right)} \frac{1}{\sin^2 \theta_p} \quad (\text{E1b})$$

$$= \frac{\alpha_p \dot{\alpha}_p}{(\alpha_p - c_1)^2 - c_2} \frac{1}{\sin^2 \theta_p}, \quad (\text{E1c})$$

where

$$c_1 = \frac{\alpha_w \cos \theta_p \cos \theta_w}{\sin^2 \theta_p}$$

$$c_2 = \frac{\alpha_w^2 \cos(\theta_p + \theta_w) \cos(\theta_p - \theta_w)}{\sin^4 \theta_p}.$$

Integrating both sides yields

$$-2\gamma t = \frac{1}{2} \log [(\alpha_p - c_1)^2 - c_2] + g(\alpha_p) \Big|_{\alpha_p(0)}^{\alpha_p(t)} \frac{1}{\sin^2 \theta_p}, \quad (\text{E3})$$

where

$$g(\alpha_p) = \begin{cases} -\frac{c_1}{\sqrt{|c_2|}} \arctan \frac{c_1 - \alpha_p}{\sqrt{|c_2|}} & \text{if } c_2 < 0 \\ \frac{c_1}{c_1 - \alpha_p} & \text{if } c_2 = 0 \\ \frac{c_1}{\sqrt{|c_2|}} \operatorname{arctanh} \frac{c_1 - \alpha_p}{\sqrt{|c_2|}} & \text{if } c_2 > 0. \end{cases} \quad (\text{E4})$$

The breakdown time can be found by setting $\alpha_p(t_b) = 0$, which results in

$$t_b = \frac{1}{2\gamma \sin^2 \theta_p} \left[\log \left(\frac{(\alpha_p(0) - c_1)^2 - c_2}{c_1^2 - c_2} \right) + g(\alpha_p(0)) - g(0) \right]. \quad (\text{E5})$$

Note that $c_1^2 - c_2$ is always non-negative.

[1] T. Tarn, G. Huang, and J. W. Clark, Modelling of quantum mechanical control systems, [Mathematical Mod-](#)

[elling](#) **1**, 109 (1980).

- [2] G. M. Huang, T. J. Tarn, and J. W. Clark, On the controllability of quantum-mechanical systems, *Journal of Mathematical Physics* **24**, 2608 (1983).
- [3] D. D'Alessandro, *Introduction to quantum control and dynamics* (CRC press, Boca Raton, FL, 2007).
- [4] H. Wiseman and G. Milburn, *Quantum Measurement and Control* (Cambridge University Press, 2010).
- [5] K. Jacobs, *Quantum measurement theory and its applications* (Cambridge University Press, 2014).
- [6] P. Brumer and M. Shapiro, *Principles of the Quantum Control of Molecular Processes* (Wiley, 2003).
- [7] C. Brif, R. Chakrabarti, and H. Rabitz, Control of quantum phenomena: past, present and future, *New Journal of Physics* **12**, 075008 (2010).
- [8] C. P. Koch, U. Boscain, T. Calarco, G. Dirr, S. Filipp, S. J. Glaser, R. Kosloff, S. Montangero, T. Schulte-Herbrüggen, D. Sugny, and F. K. Wilhelm, Quantum optimal control in quantum technologies. strategic report on current status, visions and goals for research in europe, *EPJ Quantum Technology* **9**, 19 (2022).
- [9] V. Ramakrishna and H. Rabitz, Relation between quantum computing and quantum controllability, *Physical Review A* **54**, 1715 (1996).
- [10] J. P. Palao and R. Kosloff, Quantum computing by an optimal control algorithm for unitary transformations, *Physical Review Letters* **89**, 188301 (2002).
- [11] M. Grace, C. Brif, H. Rabitz, I. A. Walmsley, R. L. Kosut, and D. A. Lidar, Optimal control of quantum gates and suppression of decoherence in a system of interacting two-level particles, *Journal of Physics B: Atomic, Molecular and Optical Physics* **40**, S103 (2007).
- [12] F. Motzoi, J. M. Gambetta, P. Rebentrost, and F. K. Wilhelm, Simple pulses for elimination of leakage in weakly nonlinear qubits, *Physical Review Letters* **103**, 110501 (2009).
- [13] M. Hsieh, R. Wu, H. Rabitz, and D. Lidar, Optimal control landscape for the generation of unitary transformations with constrained dynamics, *Physical Review A* **81**, 062352 (2010).
- [14] P. Doria, T. Calarco, and S. Montangero, Optimal control technique for many-body quantum dynamics, *Physical Review Letters* **106**, 190501 (2011).
- [15] C. Ahn, A. C. Doherty, and A. J. Landahl, Continuous quantum error correction via quantum feedback control, *Physical Review A* **65**, 042301 (2002).
- [16] M. Sarovar, C. Ahn, K. Jacobs, and G. J. Milburn, Practical scheme for error control using feedback, *Physical Review A* **69**, 052324 (2004).
- [17] M. Sarovar and G. J. Milburn, Continuous quantum error correction by cooling, *Physical Review A* **72**, 012306 (2005).
- [18] H. Mabuchi, Continuous quantum error correction as classical hybrid control, *New Journal of Physics* **11**, 105044 (2009).
- [19] R. Alicki and K. Lendi, *Quantum Dynamical Semigroups and Applications* (Springer Science & Business Media, 2007).
- [20] H.-P. Breuer and F. Petruccione, *The Theory of Open Quantum Systems* (Oxford University Press, Oxford, 2002).
- [21] P. Zanardi and M. Rasetti, Noiseless quantum codes, *Phys. Rev. Lett.* **79**, 3306 (1997).
- [22] D. A. Lidar, I. L. Chuang, and K. B. Whaley, Decoherence-free subspaces for quantum computation, *Phys. Rev. Lett.* **81**, 2594 (1998).
- [23] P. W. Shor, Scheme for reducing decoherence in quantum computer memory, *Phys. Rev. A* **52**, R2493 (1995).
- [24] A. M. Steane, Error correcting codes in quantum theory, *Phys. Rev. Lett.* **77**, 793 (1996).
- [25] D. Gottesman, Class of quantum error-correcting codes saturating the quantum hamming bound, *Phys. Rev. A* **54**, 1862 (1996).
- [26] S. Lloyd, Coherent quantum feedback, *Physical Review A* **62**, 022108 (2000).
- [27] L. Viola and S. Lloyd, Dynamical suppression of decoherence in two-state quantum systems, *Phys. Rev. A* **58**, 2733 (1998).
- [28] L. Viola, S. Lloyd, and E. Knill, Universal control of decoupled quantum systems, *Phys. Rev. Lett.* **83**, 4888 (1999).
- [29] K. Khodjasteh, V. V. Dobrovitski, and L. Viola, Pointer states via engineered dissipation, *Physical Review A* **84**, 022336 (2011).
- [30] E. Knill, R. Laflamme, and L. Viola, Theory of quantum error correction for general noise, *Phys. Rev. Lett.* **84**, 2525 (2000).
- [31] R. Blume-Kohout, H. K. Ng, D. Poulin, and L. Viola, Characterizing the structure of preserved information in quantum processes, *Physical Review Letters* **100**, 030501 (2008).
- [32] D. Lidar and T. Brun, eds., *Quantum Error Correction* (Cambridge University Press, Cambridge, UK, 2013).
- [33] M. Hecht, K. Saurav, E. Vlachos, D. A. Lidar, and E. M. Levenson-Falk, in preparation (2024).
- [34] R. M. Hirschorn, Invertibility of nonlinear control systems, *SIAM Journal on Control and Optimization* **17**, 289 (1979).
- [35] R. M. Hirschorn and J. H. Davis, Global Output Tracking for Nonlinear Systems, *SIAM Journal on Control and Optimization* **26**, 1321 (1988).
- [36] B. Jakubczyk and F. Lamnabhi-Lagarrigue, Tracking through singularities: regularity of the control, *Systems & Control Letters* **21**, 271 (1993).
- [37] Y. Chen, P. Gross, V. Ramakrishna, H. Rabitz, and K. Mease, Competitive tracking of molecular objectives described by quantum mechanics, *J. Chem. Phys.* **102**, 8001 (1995).
- [38] Z.-M. Lu and H. Rabitz, Unified formulation for control and inversion of molecular dynamics, *The Journal of Physical Chemistry* **99**, 13731 (1995).
- [39] P. Gross, H. Singh, H. Rabitz, K. Mease, and G. Huang, Inverse quantum-mechanical control: A means for design and a test of intuition, *Phys. Rev. A* **47**, 4593 (1993).
- [40] W. Zhu, M. Smit, and H. Rabitz, Managing singular behavior in the tracking control of quantum dynamical observables, *J. Chem. Phys.* **110**, 1905 (1999).
- [41] W. Zhu, J. Botina, and H. Rabitz, Rapidly convergent iteration methods for quantum optimal control of population, *J. Chem. Phys.* **108**, 1953 (1998).
- [42] W. Zhu and H. Rabitz, Quantum control design via adaptive tracking, *J. Chem. Phys.* **119**, 3619 (2003).
- [43] A. Rivas, S. F. Huelga, and M. B. Plenio, Entanglement and non-markovianity of quantum evolutions, *Physical Review Letters* **105**, 050403 (2010).
- [44] H.-P. Breuer, E.-M. Laine, J. Piilo, and B. Vacchini, Colloquium: Non-markovian dynamics in open quantum systems, *Reviews of Modern Physics* **88**, 021002 (2016).
- [45] D. Chruściński, Dynamical maps beyond markovian

- regime, *Physics Reports* **992**, 1 (2022).
- [46] I. Bengtsson and K. Życzkowski, *Geometry of quantum states: an introduction to quantum entanglement* (Cambridge University Press, 2006).
- [47] V. Kasatkin, L. Gu, and D. A. Lidar, Which differential equations correspond to the Lindblad equation?, *Physical Review Research* **5**, 043163 (2023).
- [48] P. Zanardi, Dissipation and decoherence in a quantum register, *Physical Review A* **57**, 3276 (1998).
- [49] A. Shabani and D. A. Lidar, Theory of initialization-free decoherence-free subspaces and subsystems, *Physical Review A* **72**, 042303 (2005).
- [50] D. A. Lidar and S. Schneider, Stabilizing qubit coherence via tracking-control, *Quantum Inf. Comput.* **5**, 350 (2005).
- [51] R. J. Glauber, Coherent and incoherent states of the radiation field, *Physical Review* **131**, 2766 (1963).
- [52] G. Styliaris, L. Campos Venuti, and P. Zanardi, Coherence-generating power of quantum dephasing processes, *Physical Review A* **97**, 032304 (2018).
- [53] D. Gross, Y.-K. Liu, S. T. Flammia, S. Becker, and J. Eisert, Quantum state tomography via compressed sensing, *Physical Review Letters* **105**, 150401 (2010).
- [54] S. Aaronson, Shadow tomography of quantum states, in *Proceedings of the 50th Annual ACM SIGACT Symposium on Theory of Computing*, STOC 2018 (Association for Computing Machinery, New York, NY, USA, 2018) pp. 325–338.
- [55] H.-Y. Huang, R. Kueng, and J. Preskill, Predicting many properties of a quantum system from very few measurements, *Nature Physics* **16**, 1050 (2020).
- [56] M. Hübner, Explicit computation of the Bures distance for density matrices, *Physics Letters A* **163**, 239 (1992).